Geothermics 63 (2016) 139–156

Contents lists available at ScienceDirect

Geothermics

journal homepage: www.elsevier.com/locate/geothermics

Conceptual model and numerical analysis of the Desert Peak EGS project: Reservoir response to the shallow medium flow-rate hydraulic stimulation phase

Stefano Benato[a,*], Stephen Hickman[b], Nicholas C. Davatzes[c], Joshua Taron[b], Paul Spielman[d], Derek Elsworth[e], Ernest L. Majer[f], Katie Boyle[f]

[a] Division of Hydrologic Sciences, Desert Research Institute, Reno, NV 89512, USA
[b] U.S. Geological Survey, Menlo Park, CA 94025, USA
[c] Temple University, Philadelphia, PA 19122, USA
[d] Ormat Nevada Inc., Reno, NV 89511, USA
[e] Pennsylvania State University, University Park, PA 16802, USA
[f] Lawrence Berkeley National Laboratory, Berkeley, CA 94720, USA

ARTICLE INFO

Article history:
Received 29 November 2014
Received in revised form 5 June 2015
Accepted 10 June 2015
Available online 8 July 2015

Keywords:
Desert Peak
Enhanced geothermal systems
Reservoir stimulation modeling
Induced seismicity

ABSTRACT

A series of stimulation treatments were performed as part of the Engineered Geothermal System (EGS) experiment in the shallow open-hole section of Desert Peak well 27-15 (September 2010–November 2012). These injections at variable wellhead pressures, both below and above the magnitude of the least horizontal principal stress (S_{hmin}), produced injectivity gains consistent with hydraulically induced mechanical shear and tensile failure in the surrounding rock. A conceptual framework for the overall Desert Peak EGS experiment is developed and tested based on a synthesis of available structural and geological data. These data include down-hole fracture attributes, in situ stress conditions, pressure interference tests, geochemical tracer studies, and observed induced seismicity. Induced seismicity plays a key role in identifying the geometry of large-scale geological structures that could potentially serve as preferential flow paths during some of the stimulation phases. The numerical code FLAC3D is implemented to simulate the reservoir response to hydraulic stimulation and to investigate in situ conditions conducive to both tensile and shear failure. Results from the numerical analysis show that conditions for shear failure could have occurred along fractures associated with a large northeast-trending normal fault structure located ~400 m below the injection interval which coincides with the locations of most of the observed micro-seismicity. This structure may also provide a hydrologic connection between EGS well 27-15 and injection/production wells further to the south–southwest.

1. Introduction and background

The goal of an Engineered Geothermal System (EGS) is to develop a complex and extensive fracture network in hot, initially low permeability rocks lacking commercial-scale permeability. In these systems, a desired characteristic of the generated network is a large ratio of surface area to rock volume for optimal heat exchange. When applied to operational hydrothermal reservoirs, EGS stimulations are intended to convert low-permeability unusable wells into operational injectors or producers, thereby increasing field productivity. EGS experiments to date, such as the European Soultz-sous-Forêts (Genter et al., 2009, 2013), the US Desert Peak (Chabora et al., 2012; Stacey et al., 2010; Zemach et al., 2010) and Newberry (Cladouhos et al., 2012), and the Australian Habanero (Wyborn, 2011), have typically used hydraulic stimulation techniques to enhance the permeability and connectivity of preexisting and naturally tortuous fracture networks generally found to be ubiquitous within the crust.

The Desert Peak geothermal field is a successfully operating geothermal field with ~10 MWe output located in the northern portion of the Hot Springs Mountains of northwestern Churchill County, Nevada, about 100 km northeast of Reno. Well 27-15 was selected to carry out a U.S. Department of Energy-supported EGS project with the intent of improving the hydraulic connection with the rest of the reservoir and enhancing overall injectivity (see Chabora et al., 2012 and references therein). Well 27-15 was

* Corresponding author. Tel.: +39 3317504014.
E-mail address: stefano.benato@gmail.com (S. Benato).

http://dx.doi.org/10.1016/j.geothermics.2015.06.008
0375-6505/

originally drilled to a total depth of about 1771 m, with the completed open interval (914 m–1771 m) displaying a baseline injectivity of ~0.2 gpm/psi (1.8 kg/s/MPa) (Zemach et al., 2010; Stacey et al., 2010). In 2010 it was plugged back to a total depth of about 1067 m, with the completed open-hole section available for stimulation extending from 914 m to 1067 m (here referred to as the "shallow" stimulation interval) and displaying a baseline injectivity of ~0.012 gpm/psi (0.1 kg/s/MPa) (Chabora et al., 2012; Stacey et al., 2010). In November 2012, following the shallow stimulation treatment, the well was re-completed to the original depth (1771 m), resulting in a longer open-hole section extending from 914 m to 1771 m (here referred to as the "extended" stimulation interval) which was then subjected to a final phase of full-hole stimulation (Hickman and Davatzes, 2010). Only hydraulic stimulation treatments carried out in the shallow interval of well 27-15 are considered in this study.

The first series of hydraulic stimulations conducted in the shallow open interval of Desert Peak well 27-15 from September 2010 through April 2011 led to a nearly 60-fold increase in injectivity with respect to the shallow interval baseline value (Chabora et al., 2012). This stimulation was carried out using two different fluid pressure conditions relative to the least principal stress. An initial period of shear stimulation (September 2010), which increased injectivity from ~0.011 to ~0.15 gpm/psi (0.1–1.4 kg/s/MPa) (more than one order of magnitude), was conducted as a series of steps with fluid pressures less than, or equal to, a maximum of 4.5 MPa wellhead pressure (WHP). The maximum WHP was intentionally chosen to remain below the magnitude of the least horizontal principal stress (WHP ~5.2 MPa), which was measured in this well just below the casing shoe with a mini-hydraulic fracturing test (Hickman and Davatzes, 2010). This low flow-rate phase was immediately followed by a large-volume, controlled hydraulic fracturing operation (April 2011) that lasted more than 23 days and involved high injection rates and WHP in excess of the least principal stress. This hydraulic fracturing stage resulted in a final ~0.54 gpm/psi (4.9 kg/s/MPa) injectivity (additional 4-fold increase) (Chabora et al., 2012). Temperature-Pressure-Spinner (TPS) logs show that the injected fluid exited and stimulated well 27-15 at two primary locations: (1) the bottom of the open-hole section during the low flow-rate injection phase and (2) the hydraulic fracture just below the casing shoe during the high flow-rate injection phase. Further stimulation phases – not considered here – were performed in the shallow open interval in May–June 2011 and October 2011, and in the extended open interval in January–March 2013 (Hickman et al., 2013). Stimulation operations along the extended open interval provided a final >2.1 gpm/psi (19.2 kg/s/MPa) injectivity (Hickman et al., 2013; Chabora and Zemach, 2013; Chabora and Zemach, 2013), though the analysis of this treatment is still in progress.

Throughout the EGS experiment (2010–2013), a great number of micro-earthquakes (MEQs) with magnitudes ranging from −1.0 to +1.5 were recorded between EGS well 27-15 and injection/production wells to the south-southwest, including in the proximity of injection wells 21-2 and 22-22. Some of these events appear to display a cause–effect relation between hydraulic stimulations performed in well 27-15 and deformation in the reservoir, although this relation was often complicated by injection operations being carried out simultaneously in injectors 21-2 and 22-22 (Fig. 1).

A cause–effect relation between fluid injected in well 22-22 and the occurrence of microseismicity seems evident on a few occasions such as August 2011 (Fig. 2) and March 2012 (Fig. 3). Stimulation operations were then down in EGS well 27-15 and seismic swarms followed sudden injection changes in well 22-22, and clustered in the vicinity of well 22-22. In other instances such as in April 2011, microseismic events appear to have developed as a result of stimulation treatments in well 27-15 and their hypocenters clustered in volumes closer to well 27-15 (the majority in the same depth range as a deep fault zone discussed in Section 3) (Fig. 4). For these reasons, the April 2011 stimulation phase is used for analysis and modeling purposes here (see below). Whether or not a cause–effect relation exists between fluid injected in well 21-2 and the occurrence of microseismicity is investigated and discussed below (see Section 5).

During most of the stimulation stages, including April 2011, the MEQs appear to have occurred when the greatest injectivity gains – indicating permeability development/enhancement – were observed, and for this reason it is critical to correctly understand the implications the events may have had in the stimulation treatment (Fig. 5).

Prior to the seismic network upgrade (November 2012), poor focal sphere coverage and limited constraints (signal-to-noise ratio) on the seismic velocity model made it difficult to: (1) derive the exact source mechanism for these MEQs, (2) detect events smaller than magnitude $M_w < +0.1$, and (3) define the location of individual events with precision. Regarding the detection of tensile failure during stimulation above S_{hmin}, relatively high frequency signals at the crack tip are usually produced–typically of $M \ll 0$ – which can only be detected with the use of specialized downhole instruments (Sherburn and Quinn, 2012). Thus, it is likely that the primary process generating the observed MEQ events at Desert Peak was hydraulically induced shear failure (Mode II-III) along pre-existing natural fractures and faults that were critically oriented for slip within the regional stress field ((Davatzes and Hickman, 2009; Hickman and Davatzes, 2010). Given that most of the MEQs occurred simultaneously with the greatest recorded injectivity gains, this may also indicate that some shear failure (i.e., hydro-shearing resulting in the generation of MEQs) could have contributed to reservoir transmissivity enhancement at Desert Peak (i.e., fluid supplied from well 27-15 → shear deformation → MEQs → reduction in resistance to flow → permeability gain), although this will be verified as part of a future study.

2. Objectives and roadmap

In this paper a conceptual model is developed from a comprehensive synthesis of all available geological, structural, hydrologic and seismic datasets. A hydro-mechanical, numerical framework is then implemented to test if the proposed conceptual model is generally able to reproduce observations from selected phases of the shallow stimulation experiment. The parameterization of the model is based on rock mechanics tests (Lutz et al., 2010), formation permeability computed from the integration of analyses discussed in Section 4 (Technical Approach), and stress magnitudes from a mini-hydraulic fracturing experiment.

The first goal of this study is to identify any structure that (1) appears to be spatially associated with the development of microseismicity during the various stimulation operations, and (2) may also represent a permeability conduit enabling connection to the rest of the field.

The second goal of the study is to numerically simulate whether fluid pressure diffusion in the reservoir in response to selected injection phases into well 27-15 is sufficient to induce frictional failure within the identified structures. This simulation utilizes: (a) an assessment of permeability distribution based on the integration of injectivity tests, pressure response modeling, interference test modeling and statistical Discrete Fracture Network (DFN) analyses, (b) injection rates applied to well 27-15 during the April 2011 shallow, medium flow-rate stimulation phase (Fig. 5), and (c) concurrent injection rates applied to nearby wells 22-22 and 21-2.

The April 2011 shallow, medium flow-rate phase is selected as a good candidate for numerical simulation because: (a) the timing of

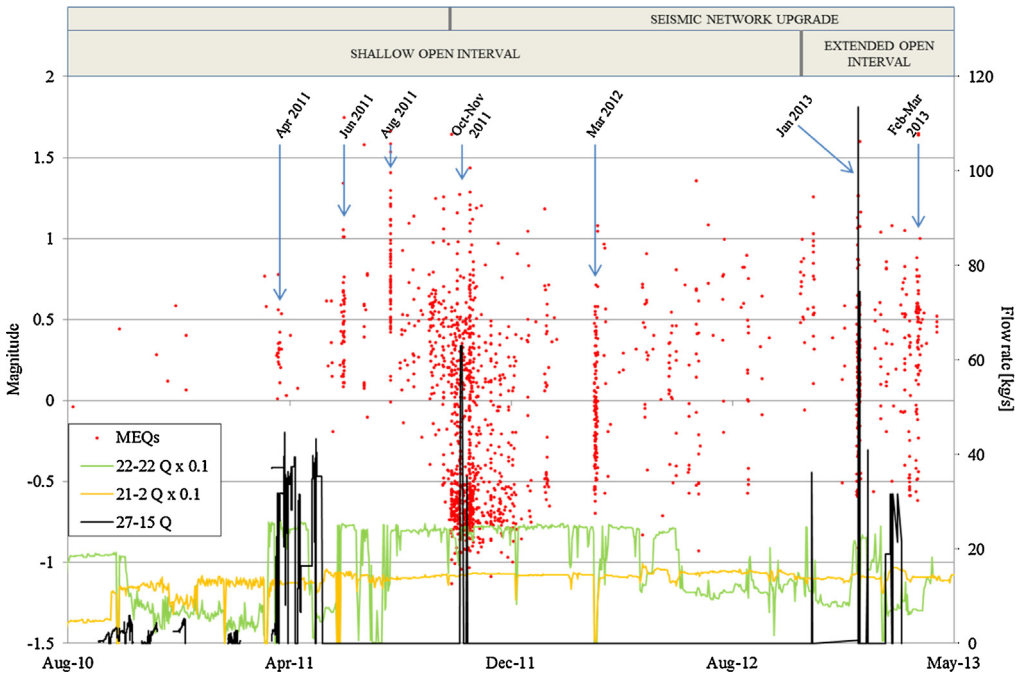

Fig. 1. Injection flow-rate history in wells 27-15, 22-22 and 21-2, and observed microseismicity throughout the EGS project. Flow-rates in wells 22-22 and 21-2 are reduced (10 times) for graphic purposes only. Different time windows in the upper part of the graph point at periods of higher density of microseismic activity. This activity appears to be associated with sudden changes in injection flow-rates in either or both wells 22-22 and 27-15.

the observed microseismic swarm appears to have coincided with the beginning of the hydraulic treatment in well 27-15 (Fig. 1), (b) the MEQs clustered in volumes closer to well 27-15 (Fig. 4), (c) the occurrence of MEQs both preceded and coincided with injectivity gains observed in well 27-15 (Fig. 5), and (d) the injection flow-rate applied to well 27-15 was relatively constant. For the purpose of this study and for simplicity, only the medium flow-rate stage is simulated here, as the overall down-hole conditions were similar to the subsequent high flow-rate stimulation phase.

3. Reservoir conceptual model

The Desert Peak geothermal field is located in the northern portion of the Hot Springs Mountains. Extensive drilling in the Desert Peak geothermal area has shown that the Hot Springs Mountains are mainly comprised of Tertiary volcanic and sedimentary rocks that lie directly on Mesozoic metamorphic and granitic basement (Faulds et al., 2010, 2012a,b; Lutz et al., 2009) (Figs. 6 and 7).

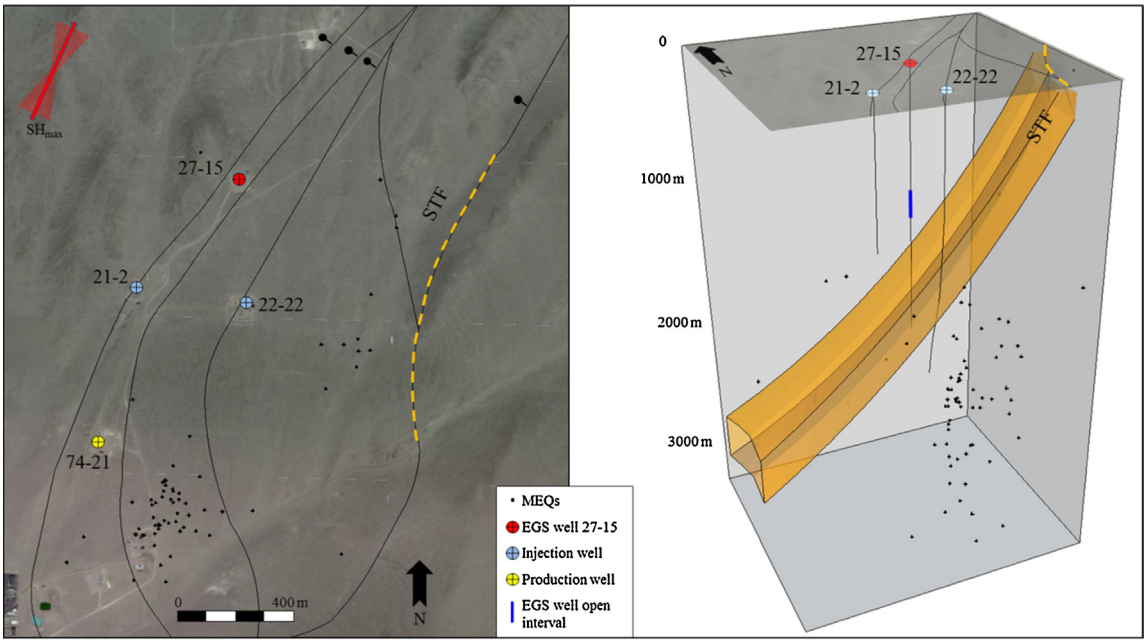

Fig. 2. Map and 3D view of the induced microseismicity observed in August 2011. Over this period, injection operations in EGS well 27-15 are down while injection in well 22-22 is being altered. The events appear located primarily around and south of well 22-22 and at the depth of a deep structural feature (STF discussed in Section 3). S_{Hmax} direction inferred from observation of borehole failures in well 27-15 (Davatzes and Hickman, 2009; Hickman and Davatzes, 2010). Black lines show surface trace of interpreted faults (Faulds et al., 2012a,b); larger black dots shown on downthrown sides of normal faults.

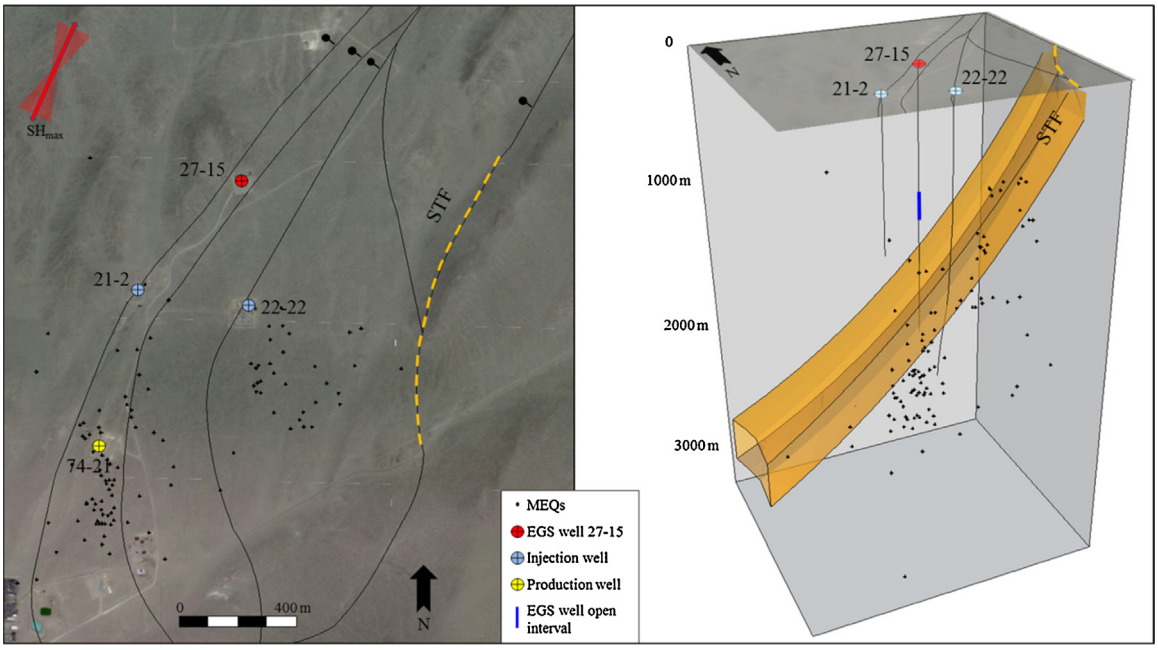

Fig. 3. Map and 3D view of the induced microseismicity observed in March 2012. Over this period, injection operations in EGS well 27-15 are down while injection in well 22-22 is being altered. The events appear located primarily around and south of well 22-22 and at the depth of a deep structural feature (STF discussed in Section 3). S_{Hmax} direction inferred from observation of borehole failures in well 27-15 (Davatzes and Hickman, 2009; Hickman and Davatzes, 2010). Black lines show surface trace of interpreted faults (Faulds et al., 2012a,b); larger black dots shown on downthrown sides of normal faults.

A combination of ~2–3 km of volcanic and sedimentary rocks makes up the Tertiary section. These are often intruded by late Miocene basalt plugs, as in the case of Desert Peak, where a large basalt plug is capped by porphyritic basalt flow (8.9 Ma). The late Miocene section of the northern Hot Springs Mountains incorporates several ash-fall deposits (i.e., Tephras). These are key markers which ease and constrain the correlation of stratigraphic units and make the offset evaluation between fault blocks possible (i.e., offset magnitude on major faults) (Stewart and Perkins, 1999; Faulds et al., 2010).

The Desert Peak geothermal field and the Northern Hot Springs Mountains lie within the NNE-trending Humboldt structural zone, which is orthogonal to the extensional direction of the Walker Lane. On a large scale, the Walker Lane is a system of dextral faults that accommodates ~20% of the relative motion between the Pacific and North American plates (Faulds and Henry, 2008).

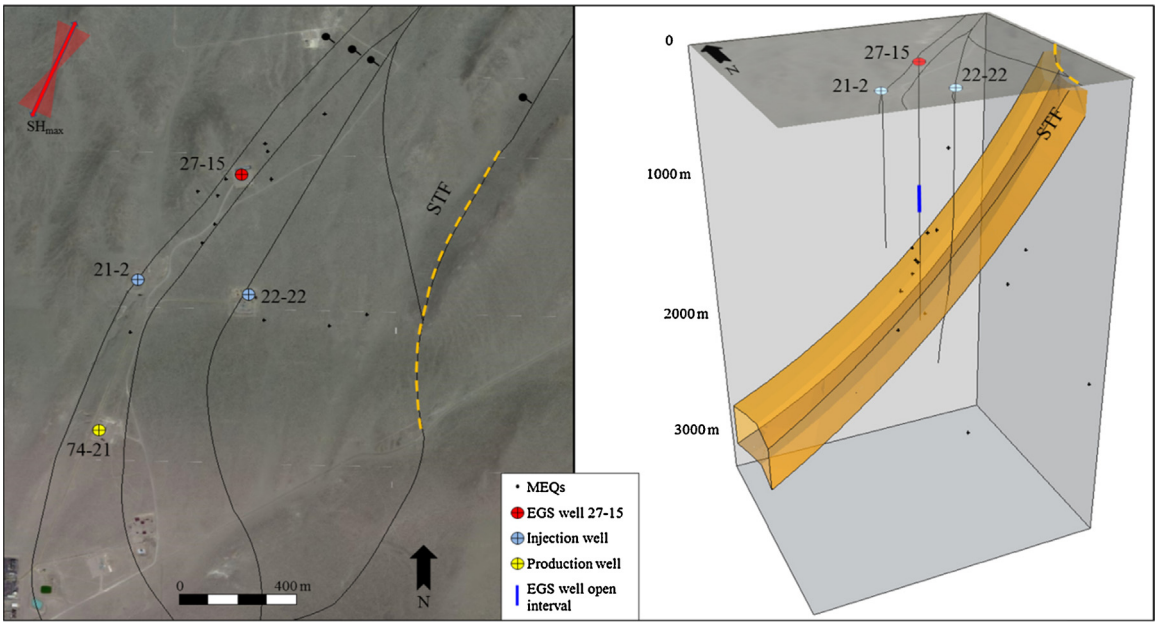

Fig. 4. Map and 3D view of the induced microseismicity observed between April 2 and April 6, 2011 (medium flow-rate phase). Over this period, the shallow open interval of EGS well 27-15 is being stimulated while injection in well 22-22 is relatively stable. The events appear primarily located around well 27-15 and at the depth of a deep structural feature (STF discussed in Section 3). S_{Hmax} direction inferred from observation of borehole failures in well 27-15 (Davatzes and Hickman, 2009; Hickman and Davatzes, 2010). Black lines show surface trace of interpreted faults (Faulds et al., 2012a,b); larger black dots shown on downthrown sides of normal faults.

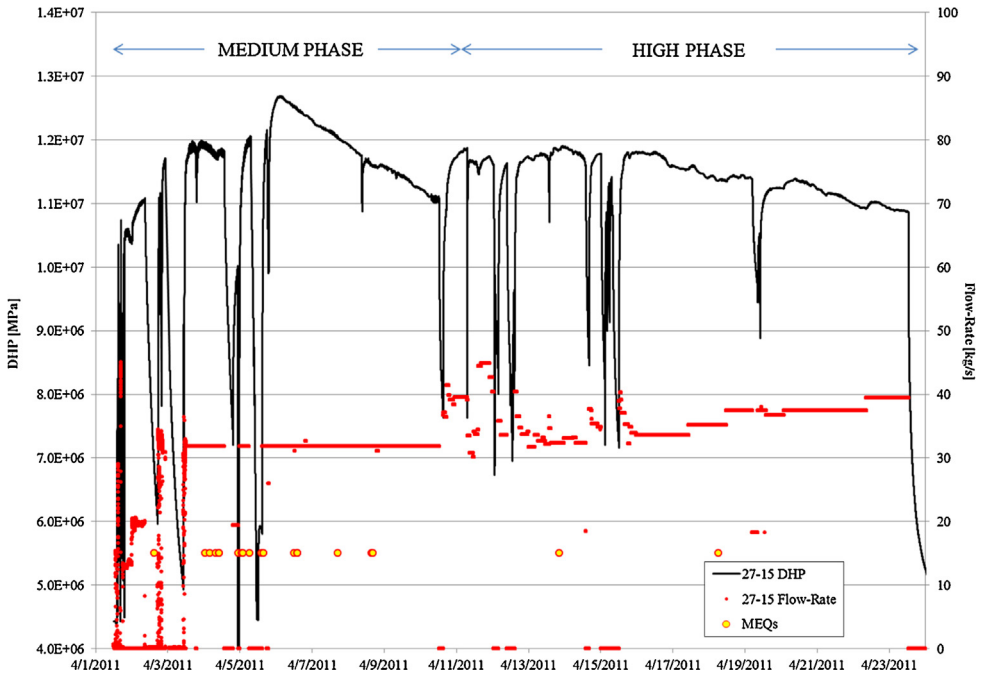

Fig. 5. Well 27-15 injection flow-rate and wellhead pressure (WHP) during the April 2011 medium to high flow-rate stimulation phases. Pressure declines under constant or increasing injection flow-rates indicate reservoir transmissivity enhancements. Microseismic activity precedes – or coincides with – the greatest injectivity gains.

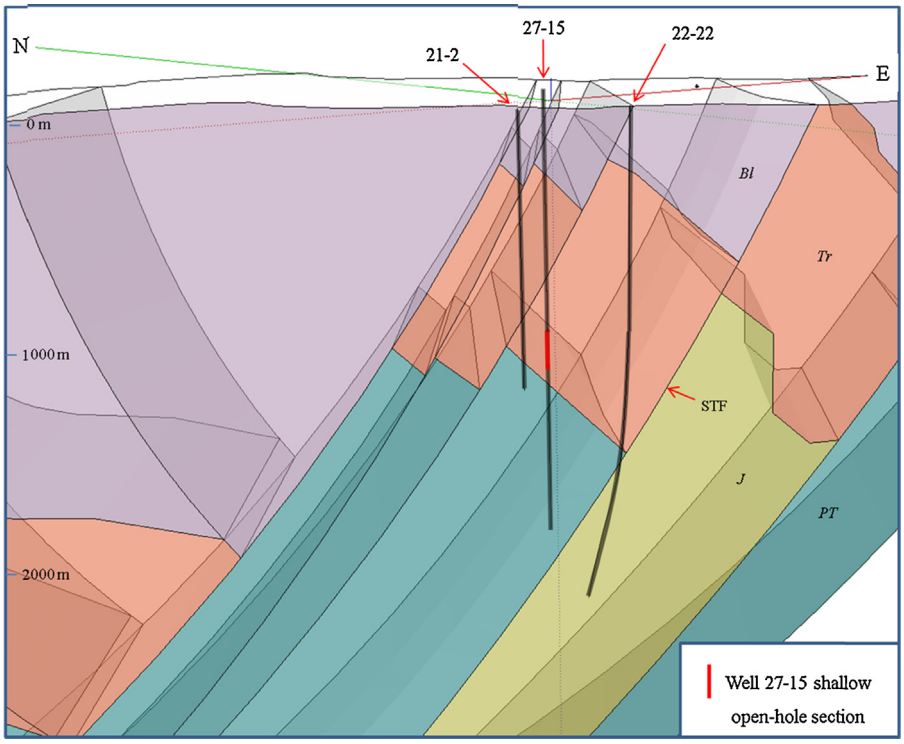

Fig. 6. Three-dimensional geological model of the EGS wellsite, derived from Faulds et al. (2010) and Faulds et al. (2012a,b) but with a simplified lithology, grouped into fewer units (Fig. 7) to facilitate conceptual modeling and numerical simulation. Unit abbreviations: J, Jurassic metamorphic basement; PT, Pre-Tertiary basement; Tr, Tertiary lavas and ash-flow tuffs; Bl, basalt lavas. Red arrow points out fault zone (STF) discussed in Section 3. (For interpretation of the references to color in this figure legend, the reader is referred to the web version of this article.)

Geodetic data indicate that about 1 cm/year of dextral motion is transferred from the north end of the Walker Lane into the WNW extension between the Sierra Nevada block and central parts of the Great Basin. This active extension and associated dilation is probably responsible for the recurrent geothermal systems in this region (Faulds et al., 2012a,b).

The dominant fault pattern trends about N25°E and appears to be related to Basin-and-Range tectonic stresses. The Humboldt structural zone may reflect both strain transfer and extension related to the Walker Lane. The most significant fault in the area is the WNW-dipping Rhyolite Ridge fault zone, which consists of several strands and steps to the left, in the vicinity of the Desert Peak

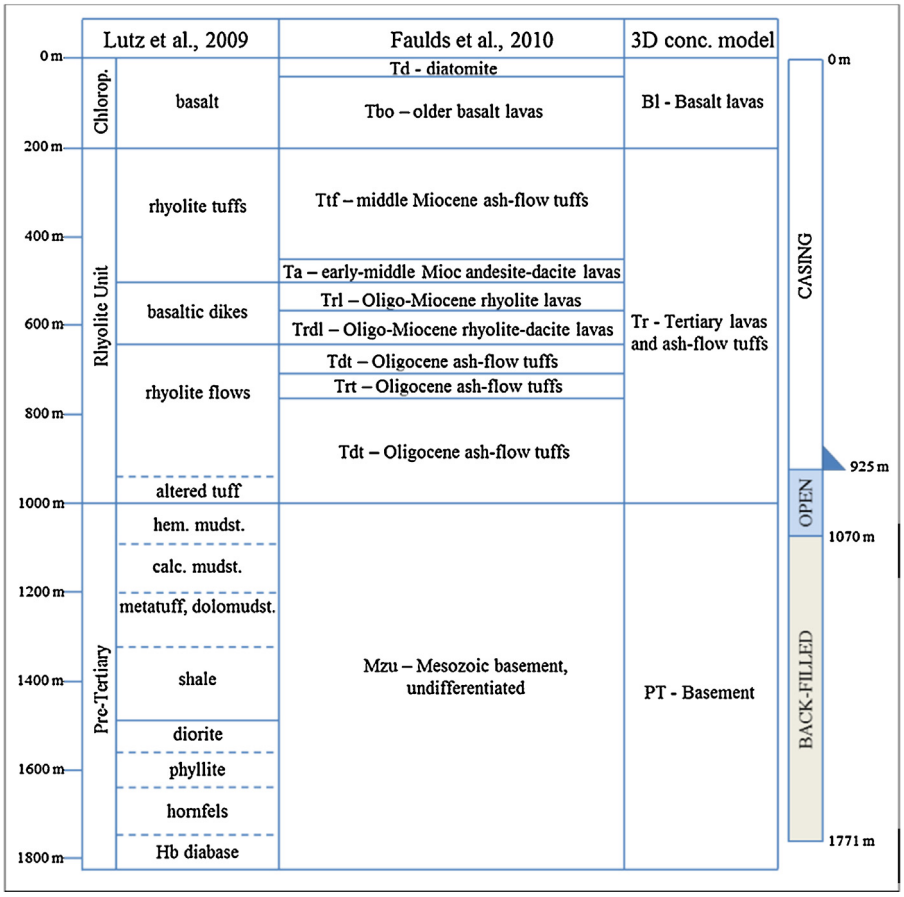

Fig. 7. Lithology correlations between available Desert Peak geological models (Faulds et al., 2010, 2012a,b; Lutz et al., 2009, 2010) and simplified lithological grouping used for the wellsite's 3D conceptual model (Fig. 6). Well 27-15 schematic diagram (shallow interval completion) also shown.

geothermal field (Faulds et al., 2010) (Fig. 8). NW-trending gravity contours across the Desert Peak field may reflect a relay ramp (Larsen, 1988) associated with southward-increasing displacement on the Rhyolite Ridge fault zone (Faulds et al., 2010). The role of the relay ramp in concentrating stress within the geothermal system based on fault geometry and local stress state is addressed in Swyer and Davatzes (2012, 2013). Kinematic data gleaned from fault surfaces indicate dip-slip normal displacement on the NNE striking faults and a WNW-trending extension direction, which is compatible with: (1) regional extension directions inferred from geodetic data (Hammond and Thatcher, 2004), (2) borehole tensile failure data and stress magnitudes from a mini-hydraulic fracturing experiment, and (3) rock densities consistent with a normal faulting stress regime from wells in the area ((Davatzes and Hickman, 2009; Hickman and Davatzes, 2010) (Fig. 8). The current stratigraphy and structural conceptualization at Desert Peak is based on original core logs and on the interpretation mainly of concealed faults. The location of structures and units may be approximate. A more detailed geological and structural analysis together with a thorough re-logging of cuttings and core (as was done in the case of the neighboring Brady's field (Faulds et al., 2013)) may provide further constraints on the Desert Peak reservoir conceptualization in future.

The most productive area in the system occupies left steps in the NNE-striking, W-dipping normal fault system (Faulds et al., 2010). Although left-stepping oblique or strike-slip faults are not required for the localization of high permeability (i.e., interaction among normal faults could also lead to dilation and locally enhanced fracture permeability in this region), the potential for high fracture density in this step-over region could enhance permeability (Faulds et al., 2010) and is consistent with modeled slips on the Rhyolite Ridge fault (Swyer and Davatzes, 2012). Tracer test returns in production well 74-21 from injection in both 21-2 and 22-22 confirm strong hydraulic connectivity in the productive area of the field (Rose et al., 2009) (Fig. 9). In contrast, tracer tests conducted by injecting into well 27-15 and sampling in well 74-21 show only a modest connection between 27-15 and the rest of the reservoir (Chabora et al., 2012).

Like many other fields, the volume of hot rock surrounding the Desert Peak geothermal field is far more extensive than the volume of hot *and* permeable rock. These circumstances drove the need for an EGS experiment that could extend the reservoir into untapped hot rock to the north of the field, creating potential new injectors and increasing the residence time of the fluid.

The orientations of the horizontal principal stresses in well 27-15 were determined through the analysis of drilling-induced tensile fractures visible in both high-temperature acoustic televiewer (ABI85) and formation micro-scanner (FMS) logs. These drilling-induced structures indicate that the azimuth of the minimum horizontal principal stress, S_{hmin}, is currently oriented $114 \pm 17°$ (corresponding to a maximum horizontal principal stress of $024 \pm 17°$) (Davatzes and Hickman, 2009). Previous analysis of stress directions from borehole failure observed in well 23-1, located 2 km E-SE of well 27-15, is in excellent agreement with stress orientations inferred from well 27-15 (Robertson-Tait et al., 2004), suggesting a regionally uniform stress field (Fig. 8).

A detailed 3D analysis of the EGS wellsite, based on the Desert Peak geological cross section and map (Faulds et al., 2010, 2012a,b),

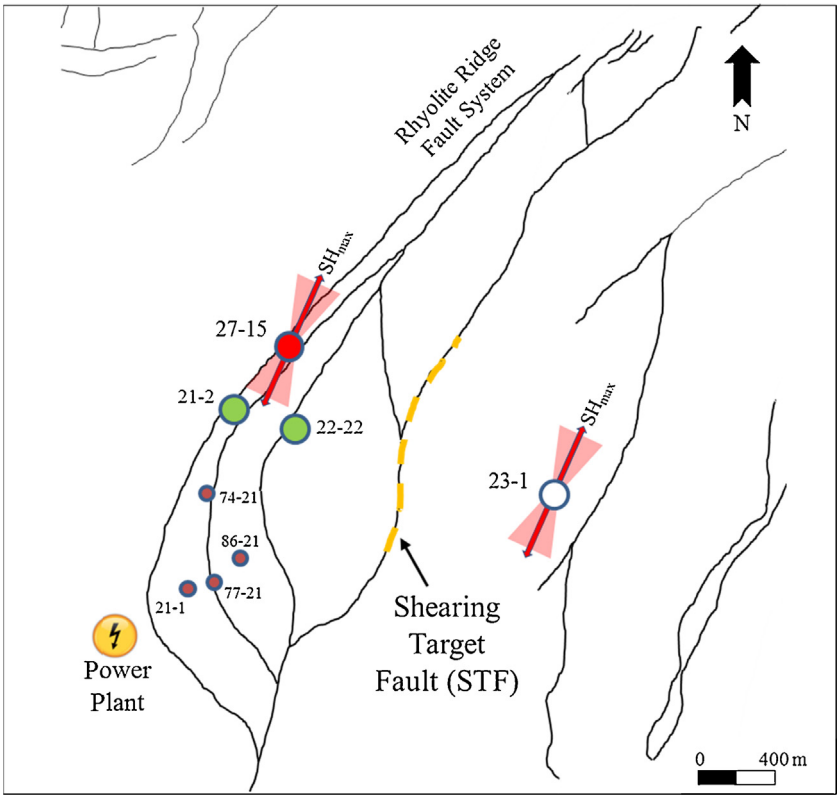

Fig. 8. Desert Peak Geothermal Field: a consistent orientation of S_{hmin} is inferred from observations of tensile fractures in wells 27-15 (Davatzes and Hickman, 2009) and 23-1 (Robertson-Tait et al., 2004). Production wells are shown in dark red, injectors in green, EGS well 27-15 in light red, unused well 23-1 in white (figure modified from Swyer and Davatzes, 2012 and Faulds et al., 2012a,b). The surface trace of the Shearing Target Fault (STF) inferred to intersect wells 22-22 and 27-15 at depth is shown with an orange dashed line. (For interpretation of the references to color in this figure legend, the reader is referred to the web version of this article.)

suggests that EGS well 27-15 and injector well 22-22 encounter the same permeable horizon at about 1400 m depth, which is consistent with a moderate inter-well connection revealed by pressure interference testing (Fig. 10) (Zemach et al., 2010) and TPS logs (Davatzes and Hickman, 2009). Significant fluid loss associated with large-aperture fractures is observed at approximately 1400 m in well 27-15 (Davatzes and Hickman, 2009) (prior to plugging back the borehole), and in well 22-22 a major feed zone is found at ~1340 m depth. The weak connectivity between wells 27-15 and 22-22 confirmed by the interference hydraulic testing (Fig. 10) (Zemach et al., 2010) may be occurring through this deeper fluid loss/feed zone (~1400 m). This horizon – striking approximately parallel to S_{Hmax} – appears to be the projection at depth of one of the main Rhyolite Ridge Fault Zone structures mapped at the surface (Figs. 8 and 11), and coincides with the depth (1400–1600 m) at which several MEQs are observed during both shallow and extended stimulation operations in well 27-15 (Figs. 4 and 19).

Therefore, a major NNE-SSW striking and WNW dipping segment of the Rhyolite Ridge Fault Zone might extend between wells 22-22 and 27-15 and establish a cross-formational hydraulic connection between these two wells (Fig. 11). This structure appears to represent a preferential flow path for fluids circulating in its vicinity and it is well oriented for shear failure within the current stress field (Hickman and Davatzes, 2010; Swyer and Davatzes, 2012). For these reasons it will be referred to as "STF" *(Shearing Target Fault)* throughout this paper. Tracer tests suggest that permeability along this structure decreases northward of the injectors (Fig. 9) or with increasing distance from the most productive area in the field (Rose et al., 2009). In the vicinity of well 27-15, the STF is sub-parallel to the main Rhyolite Ridge Fault Zone, while it appears to slightly change its orientation and steps over south toward wells 22-22 and 21-2 (Fig. 8). Among the many Rhyolite Ridge Fault strands, the STF shows one of the greatest throws, of the order of several tens of meters. Studies of surface outcrops and borehole logs of normal faults in similar settings suggest the damage zone associated to such throws may be of the order of tens of meters and even thicker where variations in dip and linkage occur (Shipton et al., 2006).

Based upon this wellsite conceptualization, we propose that some of the microseismicity observed as part of the EGS project may display shear deformation on the STF as a result of stimulation treatments carried out in well 27-15. As introduced above, injection operations into wells 21-2 and 22-22 also appear to have affected the reservoir pressurization and the development of microseismicity throughout the EGS project. In April 2011, however, the hypocenters mainly clustered in the vicinity of well 27-15 (at the depth of the STF), suggesting that a cause–effect relation between stimulation operations in well 27-15 and the development of microseismicity primarily existed during the medium to high flow-rate stimulation phases. During the April 2011 medium flow-rate phase, ~15 events (out of 18) are located in the vicinity of the STF. Taking into account the hypocenter errors, the most likely structure which generated the majority of the observed MEQs remains the STF with its surrounding damaged rock volume (Fig. 12). Toward the end of the April 2011 medium flow-rate phase, few MEQs (n. 3) appear closer to the open-hole section; their timing and location may be associated with a slight cooling/strain of the reservoir or a subordinate slip triggered by thermal damage on well-oriented sub-sets of existing natural fractures. It is difficult to define with certitude the role and origin of these (minor) events, though most of the permeability gain for this phase is observed prior to their occurrence. A more precise seismic velocity model derived from double-difference tomography (in progress) may better constrain their location and significance.

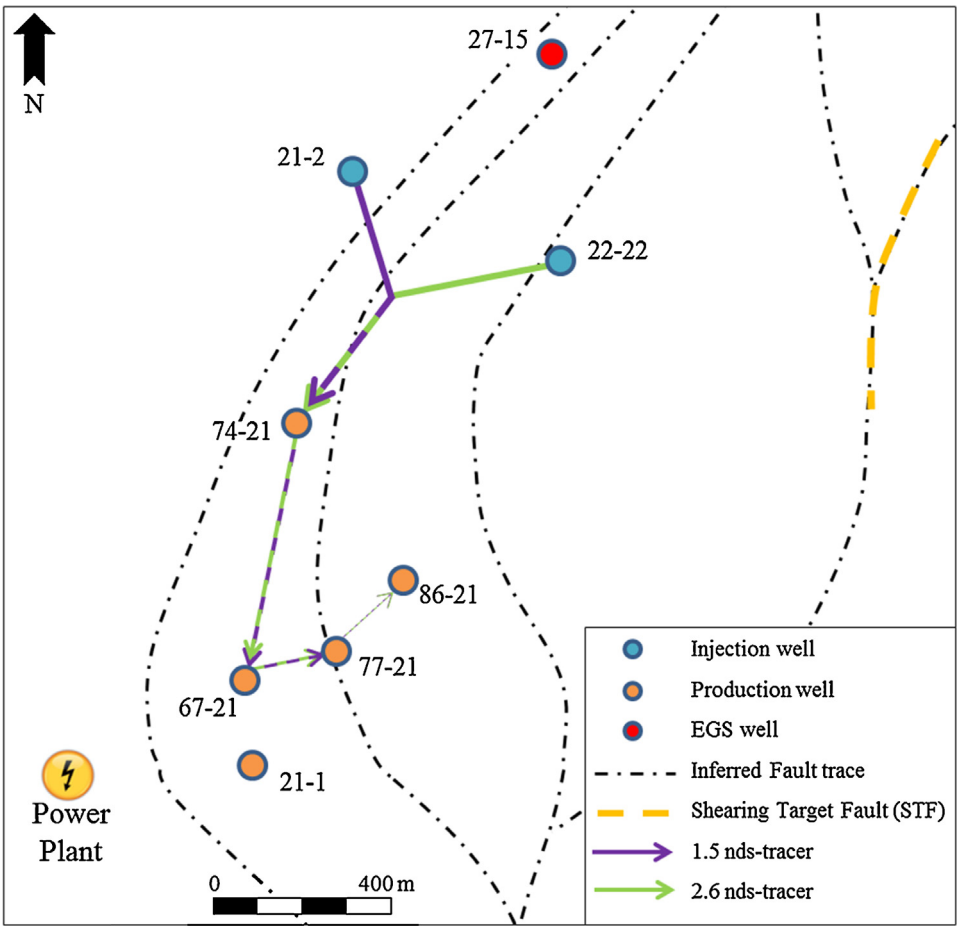

Fig. 9. Hydrologic connections (i.e., flow paths) inferred in 2009 by injecting tracers in injection wells 22-22 and 21-2 and by sampling in production wells. Results show strong returns nearest producer 74-21, and slower, weaker returns to other wells. A connection between reservoir and 22-22 occurs through the Rhyolite Unit base.
Figure modified from Rose et al. (2009) and Faulds et al. (2012a,b)

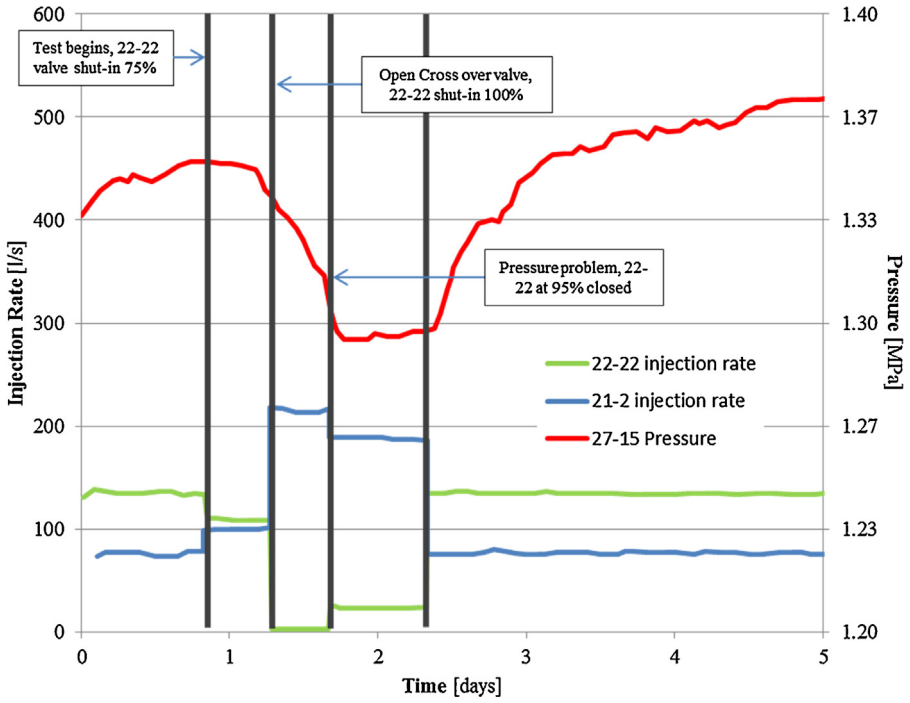

Fig. 10. 2009 interference test conducted by altering injection rates in wells 22-22 and 21-2 while observing pressure response in well 27-15 (Zemach et al., 2010). The test shows that well 27-15 is mainly (though weakly) connected with well 22-22.
Figure modified from Zemach et al. (2010)

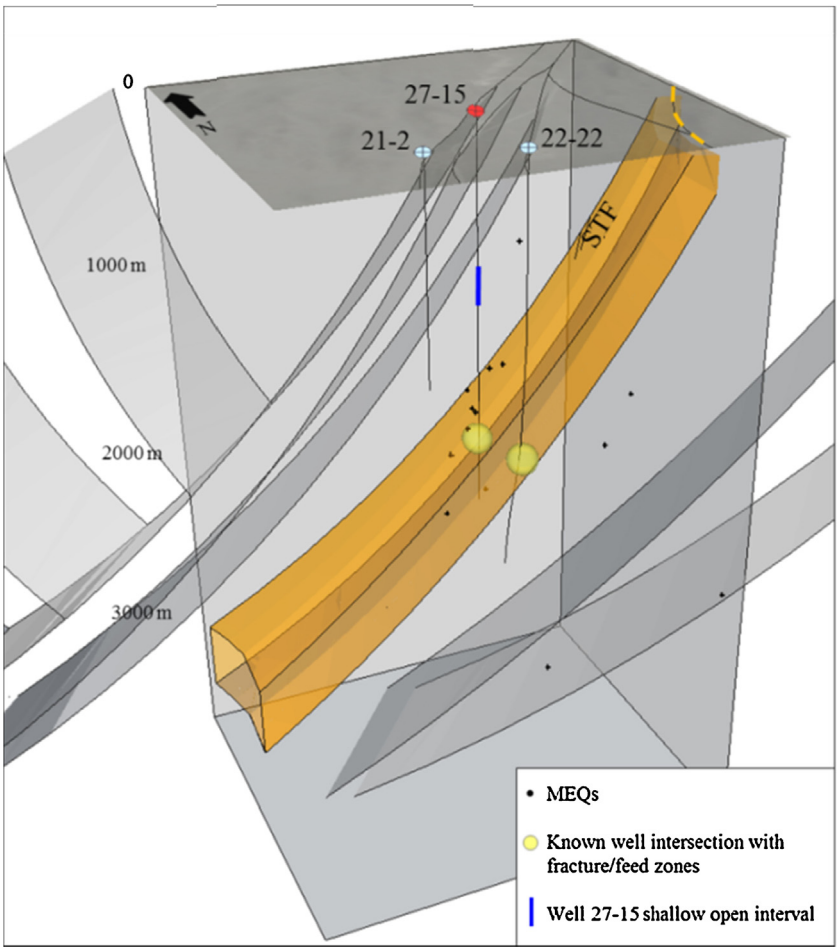

Fig. 11. Conceptual model of the major fault strands of the EGS wellsite (inferred from the Desert Peak geological cross section and map (Faulds et al., 2010, 2012a,b)). The three-dimensional geometry allows for a visualization at depth of MEQs (April 2–6 2011 - medium flow-rate, shallow stimulation) with respect to the structural setting. Both wells 27-15 and 22-22 encounter a highly fractured and permeable horizon (Shearing Target Fault "*STF*") at about 1400 m depth. Most of the MEQs are located at about 1400 m-1600 m depth, which coincides with the STF approximate projection at depth.

This conceptual model of a deep hydrologic connection between well 27-15 and wells to the SSW provides a basis on which to test potential mechanisms occurring during the Desert Peak EGS experiment and explains the relation between hydraulic treatment and observed microseismic response. Whether or not the deformation associated with the MEQs as a result of the stimulation treatment also caused the observed transmissivity enhancements needs to be demonstrated and is the subject of a parallel study. An element of note is that any hydraulically-conductive structural feature (which may provide a connection with the rest of the reservoir) potentially associated with MEQ occurrence (~400 m deeper than the shallow stimulation zone) would be isolated from the upper interval in the well because of the plug-back.

However, it is critical to understand the significance of the observed microseismicity and whether it might have highlighted potential structures to target as part of the stimulation strategy. One purpose of the modeling presented here is to test this hypothesis to see if it is consistent with known structural and stress characteristics of the EGS site and with the pore pressure generated during the April 2011 stimulation operations. In this scenario, the resulting transmission of hydraulic pressure increase within the STF is presumed to have triggered shear failure of sufficient magnitude to result in observable MEQs. This plastic deformation might in turn have enhanced permeability and fluid transmission along the STF, but – as mentioned above – this is verified in a companion study.

The STF is ~400 m deeper than the interval of fluid egress when injecting into the shallow open-hole section of well 27-15. Nevertheless, pore-pressure diffusion can interact with distant, pre-existing structures favorably oriented to failure within the regional stress field, and can initiate slip with associated microseismicity (Holland, 2011). This possibility is assessed here through coupled hydro-mechanical numerical modeling. The migration of a pressure front through pore pressure diffusion is defined by many authors as *hydraulic diffusivity* (Talwani and Acree, 1984; Nicholson and Wesson, 1990; Shapiro et al., 1999; Rothert and Shapiro, 2003; Rozhko, 2010). As a general rule, the shape of induced seismicity appears to be controlled by hydro-mechanical coupling (i.e., pressure-fracture interaction) rather than by homogeneous hydraulic diffusivity through a rock mass (Cornet, 2000).

4. Technical approach

The above conceptual model is tested for consistency against observations made before and during the Desert Peak EGS shallow stimulation. Hydro-mechanical modeling techniques are employed to assess the permeability of the triple-well reservoir (27-15, 22-22 and 21-2), and to evaluate the potential for initiating shear failure along the STF due to fluid over-pressurization.

4.1. FLAC3D coupled hydro-mechanical response model

The conceptual model is tested against the April 2011 shallow, medium flow-rate injection phase via a numerical simulation with the mechanical-flow code FLAC3D. FLAC3D is a three-dimensional

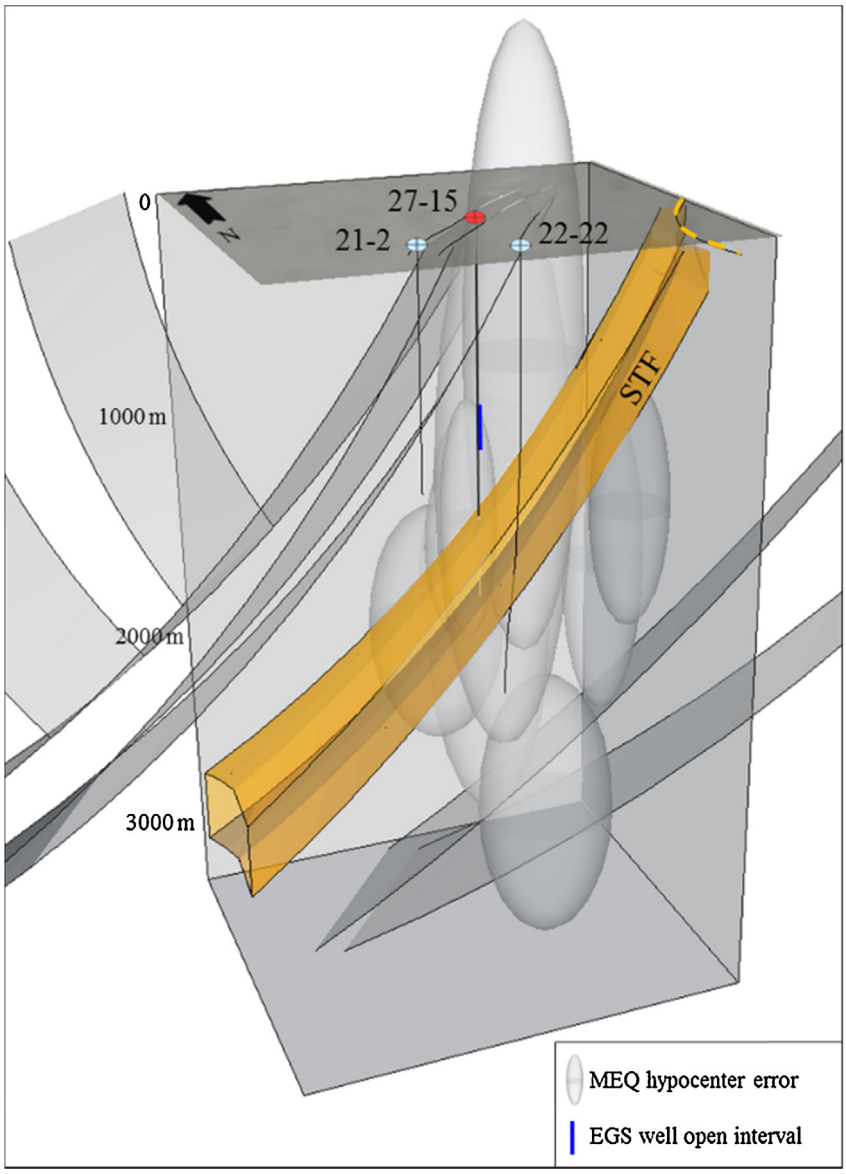

Fig. 12. Graphic representation of the hypocenter error for events observed during the April 2011 medium flow-rate stimulation phases. The structural feature most likely intersecting (thus probably generating) the majority of the MEQ hypocenter errors appears to be the STF (*Shearing Target Fault* discussed in Section 3).

explicit finite-difference program for continuum mechanics computation which also models fluid flow and its corresponding poromechanical effects (Itasca, 2011). The simulation consists of hydro-mechanically coupled calculations evaluating any expected mechanical deformation in response to injection-induced pore pressure changes within the reservoir and the STF. The FLAC3D failure envelope corresponds to a Mohr-Coulomb criterion (shear yield function) with tension cutoff (tension yield function) and the position of a stress point on this envelope is controlled by a non-associated flow rule for shear failure, and an associated rule for tension failure (Itasca, 2011). Zones in the model behave according to mechanical parameters of the material they represent and following the FLAC3D yield criterion.

As introduced above, the April 2011 shallow, medium flow-rate stimulation phase is a good candidate for this simulation. Therefore, the pressure diffusion model through the reservoir is tuned to cause plastic deformation that could produce MEQs in response to the injection rates applied into 27-15, 22-22 and 21-2 during this phase. Sufficient pressure to reduce the effective normal stress must be communicated to the STF to satisfy the conditions for Mohr-Coulomb failure. The relative pressure perturbation effect from injection into each different well is investigated as part of the modeling exercise presented below.

As a general rule, the simplest geometry compatible with the geology and hypotheses being tested is used to define the FLAC3D model, consistent with the reproduction of key physical processes. In the simplified representation of the wellsite, the model comprises a uniform background formation, three injectors (wells 27-15, 22-22 and 21-2) and a fault zone (STF) dipping ~70° and located ~400 m below the actual 27-15 injection point (Fig. 13). The fault zone (STF) in the model is set to be about 100 m thick in order to account for its damage zone (given a fault throw greater than several tens of meters (Shipton et al., 2006). The grid is aligned with the Rhyolite Ridge Fault Zone and the STF (i.e., with the known tectonic stresses), thus rotated ~20° clockwise from the north. In the vicinity of well 27-15 the STF is represented sub-parallel to the main Rhyolite Ridge Fault Zone, while it is slightly rotated toward wells 22-22 and 21-2 to account for the apparent step-over discussed in Section 3 (Figs. 8 and 13). The model domain extends for 3000 m in the *x*-direction, 1800 m in the *y*-direction and 2600 m

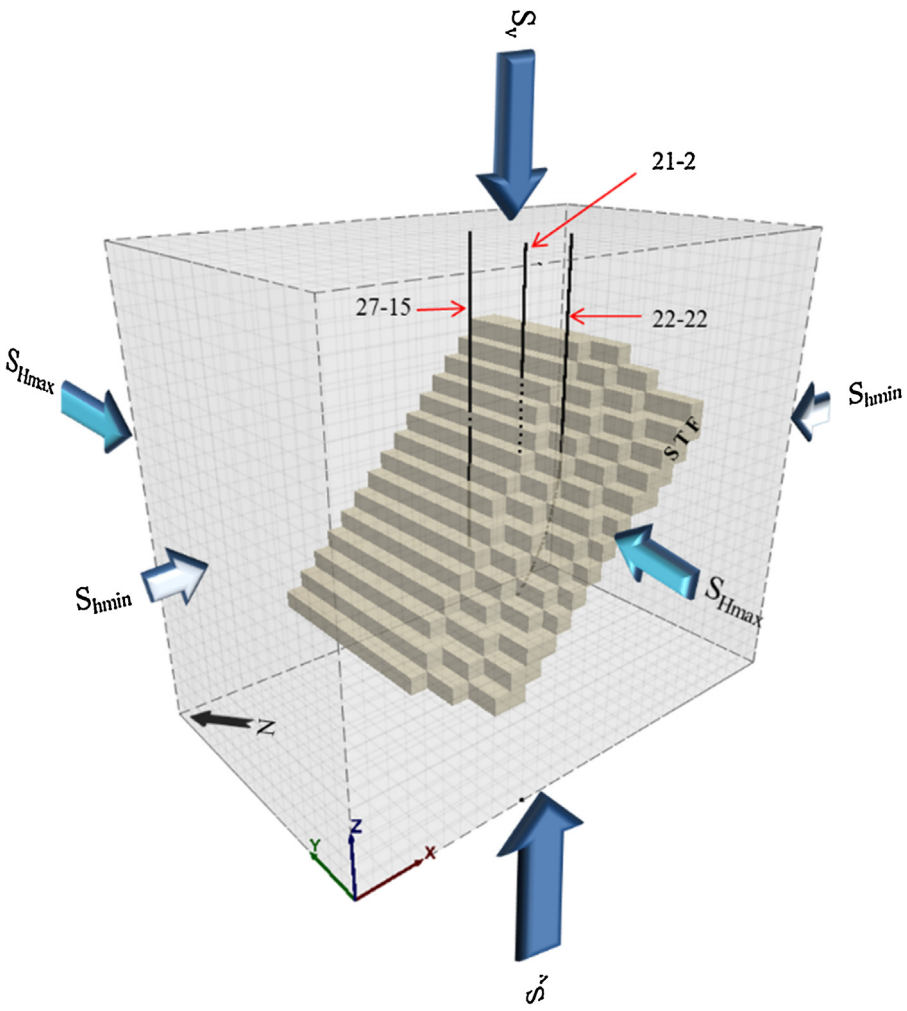

Fig. 13. FLAC3D model construction. The model comprises a uniform background formation, three injectors (27-15, 22-22 and 21-2) and a ~100 m thick NNE-striking, WNW-dipping (70°) Shearing Target Fault (STF). Stresses are applied according to the normal faulting regime observed in the field and using the measured magnitude of S_{hmin} (i.e., $\sigma zz > \sigma yy > \sigma xx$).

in the *z*-direction. The grid is discretized into regular cubic zones (100 m per side). The model – as well as the STF – are currently assumed to be single-porosity media. Parallel modeling exercises involving coupling with TOUGHREACT (Xu et al., 2004) adopt a dual-porosity conceptualization. A phreatic surface is initialized at a depth of 118 m. Below this surface pore pressures follow a linear gradient once the initial force-equilibrium state is reached, i.e., a force-equilibrium is assumed when the maximum unbalanced force and velocity vectors at each gridpoint are small compared to the representative zone forces in the problem.

For simplicity and numerical purposes, the lithological units described in Section 2 are grouped into rock types: *a* corresponding to the basement and rhyolite units (background rock mass), and *b* representing the STF (Table 1). The mechanical parameters used in the model are derived from rock mechanical tests conducted on selected core samples representative of the stimulation interval in well 27-15 (Lutz et al., 2010). In order to appropriately model the propensity for frictional failure in a fractured reservoir, Mohr-Coulomb properties (friction and cohesion) evaluated from residual compressive strength measurements (residual values after failure) for the Rhyolitic and Metamorphic Basement Units are averaged and assigned to rock type *a*. Elements pertaining to the STF are set with a lower friction angle of 28° and zero cohesion, as in situ stress measurements in a variety of tectonically-active geological settings suggest that fracture planes well oriented with respect to the stress field are generally cohesionless (Hickman, 1991; Townend and Zoback, 2000) (Table 1).

Table 1
Mechanical properties used in the FLAC3D hydro-mechanical model (from Lutz et al., 2010). In the model, tensile strength of the material never exceeds the maximum value given by $\sigma^{\tau}_{max} = c/\tan\varphi$, where c is cohesion and φ friction angle.

Parameter	Background (rock type a)	STF (Rock type b)
Density [g/cm^3]	2.7	2.7
Shear modulus [MPa]	1.0E+04	1.0E+04
Bulk modulus [MPa]	2.6E+04	2.6E+04
Friction angle [°]	39	28
Cohesion [MPa]	4.2	0
Tensile strength [MPa]	1.0E+04	1.0E+04

The model is set with permeable boundary conditions, i.e., the pressure remains constant at the boundaries. Velocity and displacement are fixed at the bottom and sides of the model. Permeability is initialized as explained in Section 3. Consistent with the normal faulting regime observed in the field and using the measured magnitude of S_{hmin} (Hickman and Davatzes, 2010), *xx*, *zz* and *yy* stress components vary with depth following the relations among S_{hmin}, S_{Hmax} and S_v (vertical overburden): $S_{Hmax} = (S_{hmin} + S_v)/2$, and $S_{hmin}/S_v \approx 0.61$ (Hickman and Davatzes, 2010). At the depth of the injection zone the following stress values apply: $S_v = 24.6$ MPa, $S_{hmin} = 15.0$ MPa, $S_{Hmax} = 19.8$ MPa. A Mohr-Coulomb plasticity

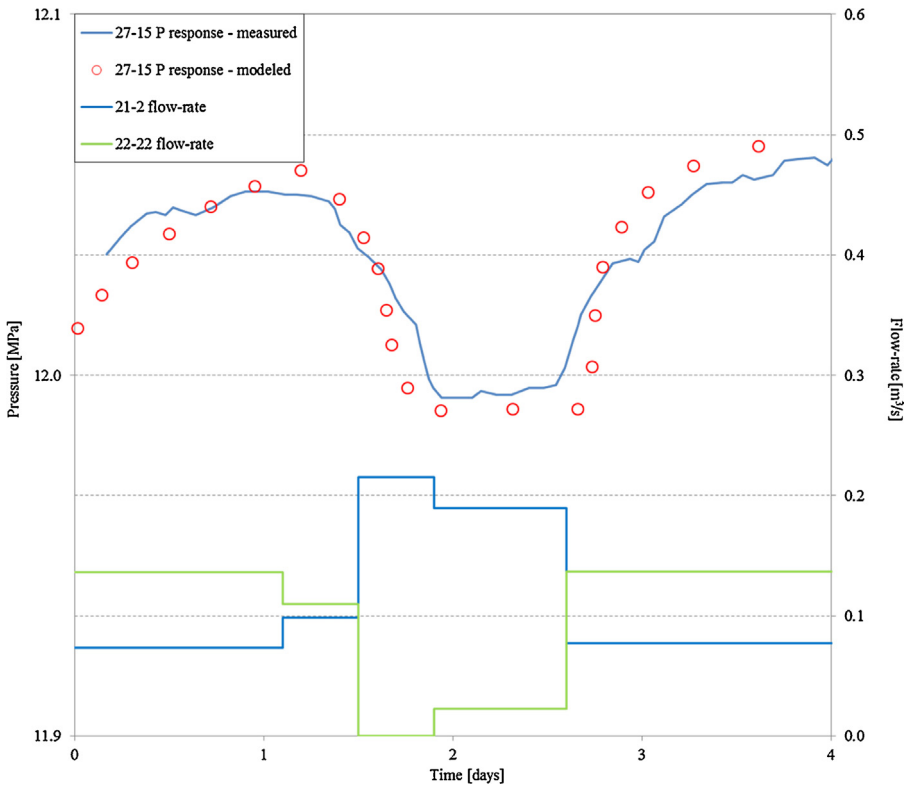

Fig. 14. FLAC3D simulation of the 2009 interference test (Zemach et al., 2010) (Fig. 10): pressure response observed in well 27-15 while varying injection flow-rates in wells 22-22 and 21-2. The good fit between measured and modeled pressure curves suggests the permeability field is appropriately initialized.

constitutive model is set in FLAC3D to properly represent the onset of shear (frictional) failure. The failure envelope for this constitutive model corresponds to a Mohr-Coulomb criterion which is expressed in terms of principal stresses σ_1 and σ_3. For the Mohr-Coulomb plasticity model, the required properties defined for each material are: (1) bulk and shear moduli, (2) friction and dilation angles, (3) cohesion and (4) tensile strength. The constitutive behavior and associated material properties affect the model response as well as stress perturbations caused by fluid injection (Itasca, 2011).

Boundary and initial conditions define the in situ state (i.e., before a change or disturbance is introduced by injection). An initial equilibrium state – during which gravitational stresses develop – is obtained by running the model under dry conditions and through mechanical-only calculations. A second equilibration is then calculated by running flow calculations in parallel with the mechanical modeling, in order to capture the effects of solid-fluid interaction. An alteration is then made (e.g., fluid injection resulting in pore pressure change), and the resulting mechanical response throughout the model is computed. A prescribed volumetric inflow of fluid is assigned to wells 27-15, 22-22 and 21-2 to define the principal fluid sources in the model.

The fluid-mechanical interaction is solved with a coupled approach where the mechanical process is the "slave" module to the master fluid flow process, given that the stress perturbation is pore-pressure driven.

The model simulates the flow-rates injected in: (a) wells 21-2 and 22-22 over the March 24–April 10, 2011 period, and (b) well 27-15 over the April 01–April 10, 2011 period. This is done in order to correctly reproduce reservoir pressurization conditions not only during, but also prior to the stimulation treatment of well 27-15. The average volumetric flow-rates applied to the corresponding open-hole sections of the wells are summarized in Table 2.

Table 2
Average volumetric flow-rates applied to the corresponding open-hole sections in the model when simulating the April 2011 medium flow-rate phase.

Well	Avg. flow-rate [m^3/s]	Open-hole section [m] (measured depth)
21-2	0.13	618–972
22-22	0.24	1270–2051
27-15	0.032	914–1067

4.2. Assessment of reservoir permeability

The incorporation of injectors 22-22 and 21-2 in the modeling study of EGS well 27-15 requires a permeability assessment for both the formation comprising well 27-15 (*lower k*) and that around wells 22-22 and 21-2 (*higher k*).

The permeability of the triple-well reservoir considered in this study (27-15, 22-22 and 21-2) is estimated by integrating: (1) pre-EGS baseline permeability-thickness values from injection tests carried out for both the shallow and the extended open interval of well 27-15 (Stacey et al., 2010), (2) detailed, single-wellbore FLAC3D simulation of known wellhead pressure responses to fluid injection, (3) FLAC3D simulation of the 2009 interference test (Zemach et al., 2010) (Fig. 10), and (4) DFN analysis from a companion paper (Benato et al., 2013).

The permeability of the formation surrounding wells 21-2 and 22-22 is estimated by running single-wellbore FLAC3D simulations of the wellhead pressure response to fluid injection, which is best matched using a permeability of ~5.6e−13 m^2.

As per the formation surrounding well 27-15, pre-EGS injection tests revealed a permeability of 2.0e−15 m^2 (5600 md-ft) and of 1.2e−16 m^2 (60 md-ft) for the extended (850 m) and shal-

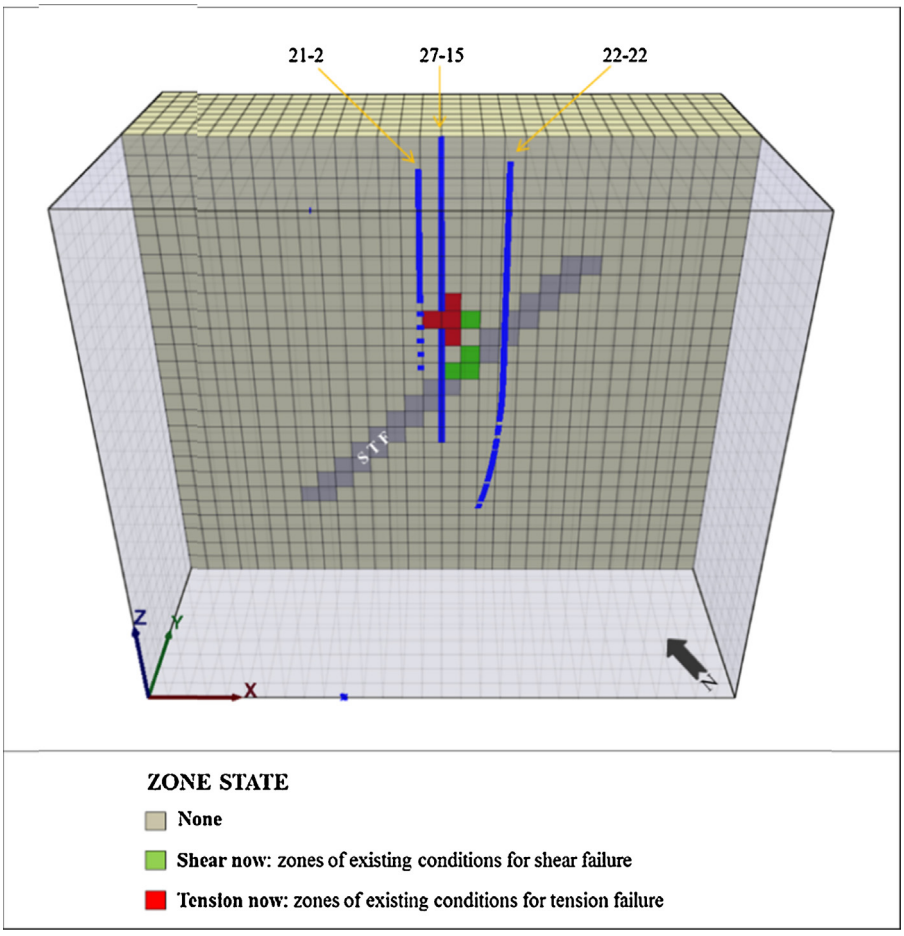

Fig. 15. FLAC3D coupled hydro-mechanical simulation and mechanical response as a result of fluid injection during the April 2011 medium flow-rate stimulation phase. FLAC3D displays conditions for: (1) tension failure in volumes surrounding the well 27-15 open-hole section (in agreement with fluid pressures exceeding S_{hmin}), and (2) shear failure mainly at STF depths. Limited conditions for shear failure also develop in the vicinity of the well 27-15 open interval.

low (150 m) open intervals, respectively (Stacey et al., 2010). The lower permeability in the shallow interval is in agreement with the range of magnitudes obtained from measurements on core plugs under ambient stress conditions (Rozhko, 2010). The higher permeability displayed by the extended interval is assumed here to be the result of higher hydraulic conductivity in the STF (intersected by this interval). With this in mind, the 2009 (pre-EGS) interference test (Zemach et al., 2010) is simulated in FLAC3D by applying the permeability values described above to the background formation of well 27-15 ($1.2e{-}16\ m^2$) and of wells 21-2 and 22-22 ($5.6e{-}13\ m^2$). The STF permeability is then adjusted until a good fit with the pressure response observed during this test is reached. The best results are obtained when the STF permeability is $\sim 3.0e{-}14\ m^2$. The ratio among the three components k_x, k_y and k_z of the permeability tensor computed through DFN analysis in a previous study (Benato et al., 2013) is maintained and applied to the background formation surrounding well 27-15 to retain the anisotropic permeability distribution of the wellsite (Table 3). The triple-well simulation results of the 2009 interference test – carried out by altering injection flow-rates in wells 21-2 and 22-22 and observing the pressure response in well 27-15 – suggest that the defined permeability is consistent with the reproduction of the field characteristics (Fig. 14).

An element of note is that the April 2011 stimulation (considered in this study) follows the September 2010 phase, during which the permeability of the formation surrounding the well 27-15 shallow interval is considerably improved (Chabora et al., 2012). Here we estimate this enhanced permeability through single-wellbore FLAC3D simulations of the wellhead pressure response observed during the initial steps of the April 2011 medium flow-

Table 3
Summary of permeability values estimated for: (a) well 27-15 background formation, (b) volumes with permeability enhanced as part of the September 2010 low-flow-rate phase, (c) formation surrounding wells 22-22 and 21-2, and (d) Shearing Target Fault (STF). Anisotropic permeability – derived from DFN analysis (Benato et al., 2013) – is used for the well 27-15 background formation.

	Model hydraulic parameters			
	$k\ [m^2]$	ky	kx	kz
(a) Well 27-15 background formation	1.2E−16	1.83E−16	2.50E−17	6.16E−17
(b) September 2010 enhanced k	1.1E−14	–	–	–
(c) Wells 22-22 and 21-2 formation	5.6E−13	–	–	–
(d) Shearing Target Fault (STF)	3.0E−14	–	–	–

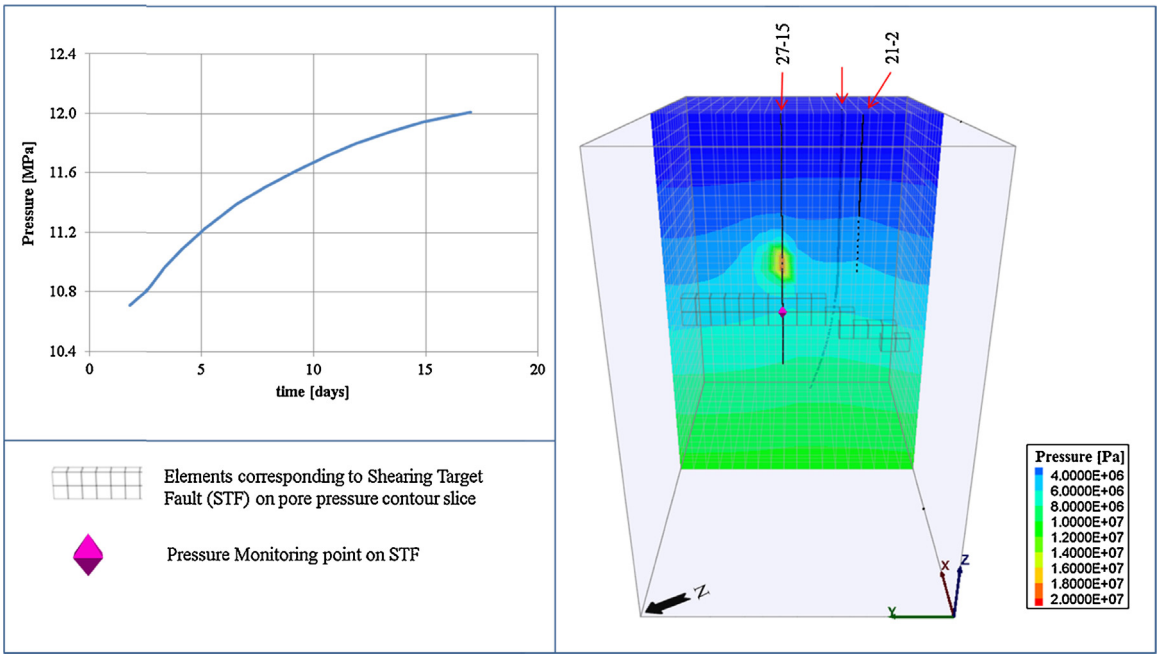

Fig. 16. The April 2011 medium flow-rate stimulation phase is modeled with FLAC3D by simulating fluid injection in the well 27-15 shallow open-hole section and in wells 21-2 and 22-22. Pore pressure diffusion from the well 27-15 shallow open interval combines with pressure from concurrent injection in wells 21-2 and 22-22 – increasing the pore pressure at the depth of the STF by about 1 MPa. The modeled pressure in the immediate vicinity of the wellbore is somewhat higher than field observations because (1) the modeled pressure is slightly deeper than the measured, downhole pressure, and (2) transient permeability is not considered here. Transient permeability is in the author's ongoing FLAC3D-TOUGHREACT study.

rate phase. We do so by increasing the pre-EGS permeability value ($1.2e{-}16\,m^2$) in the formation surrounding the well 27-15 shallow open interval to ~$1.1e{-}14\,m^2$, which provides an adequate match with the observed overpressure. This value is integrated into the permeability field described above to set-up the initial conditions for the April 2011 phase simulation.

5. Results

Under the April 2011 shallow, medium flow-rate stimulation conditions, FLAC3D coupled hydro-mechanical simulations display conditions for shear failure pertaining to the stimulated reservoir volumes (i.e., around the open interval and at the depth of the STF). In the model, failure is manifested as a contiguous series of actively failing zones in which stresses satisfy the FLAC3D yield criterion (as defined in Section 4.1) (Figs. 15 and 18A). Conditions for tensile failure also develop in volumes surrounding the well 27-15 open-hole section, in agreement with injection-induced fluid pressures (~20 MPa) exceeding S_{hmin} (~15 MPa) during the medium flow-rate phase (Fig. 15).

With the parameterization listed in Table 1, results show that shear failure may occur at the depth of the STF (Fig. 15) where injection-induced pore pressure increases by more than 1 MPa as a result of the stimulation operation (Fig. 16).

Injection-induced pore pressure diffusion computed by FLAC3D is also tested with a Mohr-Coulomb analytical approach to verify if the resulting pressure incremental could satisfy conditions for shear failure on well-oriented sets of fractures at the depth of the STF. The Mohr-Coulomb analysis confirms that this pressure increase within the STF would create critical conditions for shear deformation on well-oriented, cohesionless fractures (Fig. 17).

With the current model configuration, simulation results show that shear deformation at the depth of the STF and toward well 27-15 is enhanced when both wells 27-15 and 22-22 are actively injecting fluid (Fig. 18B). Pore pressure diffusion from concurrent injection in wells 27-15 and 22-22 combine, further destabilizing the STF. Fluid injection simulation into well 22-22 alone or simultaneously into wells 22-22 and 21-2 is insufficient to develop conditions for shear failure. Fluid injection into well 21-2 does not seem to impact the development of deformation on the STF.

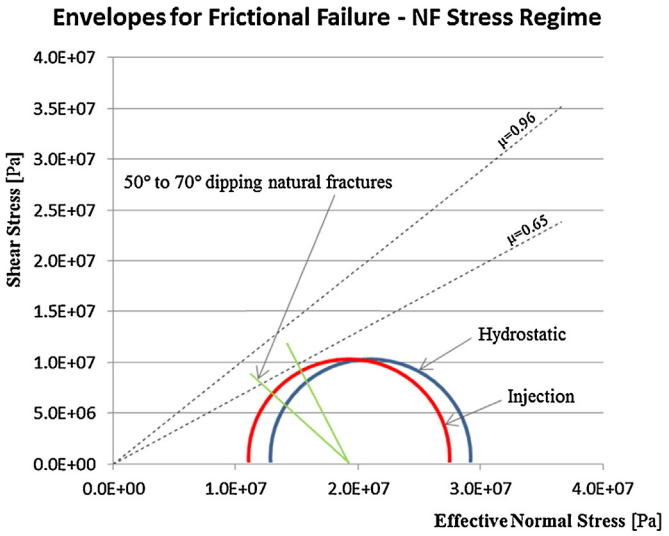

Fig. 17. Normal-stress regime Mohr circles showing shear and effective normal stress at ~1400 m depth (location of MEQs and STF) under: (1) hydrostatic conditions (blue circle) defined assuming a groundwater level 118 m below surface, and (2) April 2011 medium flow-rate injection-induced conditions (red circle) derived from FLAC3D simulation (Fig. 16). Frictional failure lines are based on the sliding friction coefficient derived from rock sample laboratory testing from surrounding geological units (Lutz et al., 2010). In situ natural and cohesionless fractures at the depth of the STF are close to being critically stressed for shear failure under the April 2011 medium flow-rate phase conditions. (For interpretation of the references to color in this figure legend, the reader is referred to the web version of this article.)

Shear failure distribution shown in the modeling results is in agreement with the microseismicity observed during the April 2011 phase, which appears to cluster mainly in the same depth

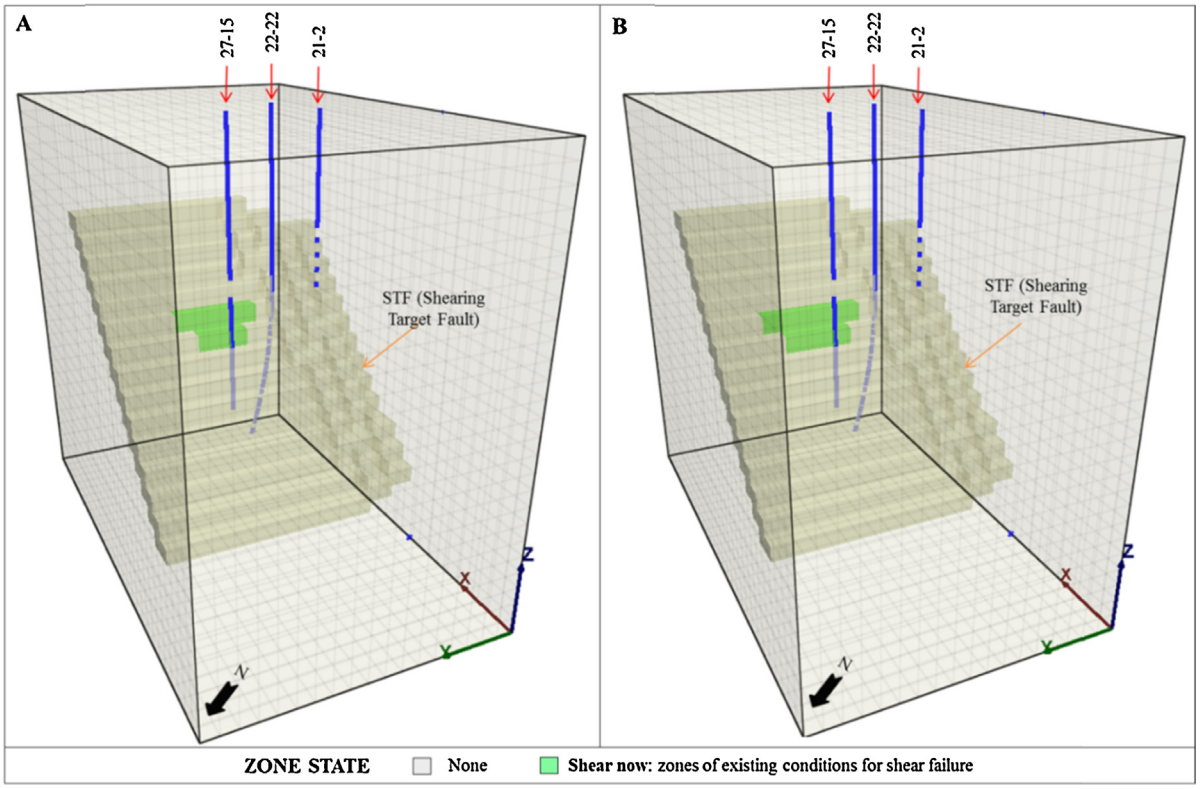

Fig. 18. FLAC3D coupled hydro-mechanical simulation and mechanical response resulting from injection-induced pressure diffusion generated during the April 2011 medium flow-rate stimulation phase. The results display conditions for shear failure developing on the STF in the case of: (A) injection in well 27-15 alone (or concurrent with injection in well 21-2), and (B) concurrent injection into wells 27-15 and 22-22. When the April 2011 phase injection rates are simulated, conditions for shear failure develop on the STF in the vicinity of well 27-15, where the bulk of microseismicity is observed during this phase. Fluid injected in well 21-2 does not seem to influence the development of shear deformation with the current model configuration.

range of the STF below the shallow stimulated interval of well 27-15 (Fig. 4).

6. Discussion and conclusions

In order to define a possible connection between stimulation operations in well 27-15 and the development of the observed MEQs, as well as to offer a possible explanation for their deep location, the present study analyzes: (1) 3D site-specific geometry of the key structures involved in the experiment, (2) assessment of permeability distribution based on integrating DFN analysis, injectivity tests, pressure response modeling and interference test modeling, (3) hydro-mechanical simulation of pore pressure diffusion and resulting mechanical deformation consistent with the activation of hydraulically-induced shear failure in the reservoir.

The MEQ clusters observed during the EGS experiment are mainly used for structural identification purposes. The numerical simulation honors the April 2011 medium flow-rate injection phase, when MEQs appear grouped together in volumes closer to well 27-15, if compared to microseismic swarms observed at other times.

The mechanical response of the reservoir that results from injection into the shallow open-hole section of well 27-15 (April 2011 conditions) is simulated in FLAC3D to verify possible conditions for deformation and shear failure initiation. The conceptual and numerical modeling results reveal that pore pressure diffusion to depths below the stimulation interval during the April 2011 EGS shallow injection phase in well 27-15 – especially if combined with injection operations in well 22-22 – can lead to pressurization and poromechanical stressing of the STF.

Modeling results display shear failure affecting reservoir volumes at depths associated with the STF. The location of zones indicating conditions for shear failure is in agreement with the microseismicity distribution observed during this phase: mainly clustered at the depth of – and aligned with – the STF. The model suggests that rapid and considerable changes in the injection flow-rates cause a sudden modification of the stress state, destabilizing the STF considerably.

These results (i.e., pressure diffusion → conditions for shear failure on the STF) support the proposed STF-based conceptual model framework, which correctly reproduces the cause–effect relation between well 27-15 stimulation operations and the development of microseismicity – especially when concurrent with injection in well 22-22. This interaction between well 27-15 and well 22-22 is in agreement with both (a) the 2009 pressure interference test, which suggests that well 22-22 can deliver some pressure toward well 27-15, and (b) the absence of microseismicity in the vicinity of well 27-15 prior to the stimulation treatment. This is consistent with the concept proposed in other experiments, e.g. Soultz, where simultaneous injection into adjacent wells (or "*focused stimulation*") delivered the most effective stimulation and hydraulic connection development (Schlinder et al., 2010; Baria et al., 2006; Hettkamp et al., 2004).

The FLAC3D simulation indicates localized pore pressure increases up to 1 MPa at the depth of the STF and suggests that effective stress changes induced by these fluid pressure increases are sufficient to produce slip (and possibly microseismicity) within the STF. This is also confirmed by evaluating the resulting effective pore pressure through a Mohr-Coulomb analysis (Fig. 17). Both numerical (coupled hydro-mechanical) and analytical (Mohr-Coulomb) results support the existence of regions in the STF which

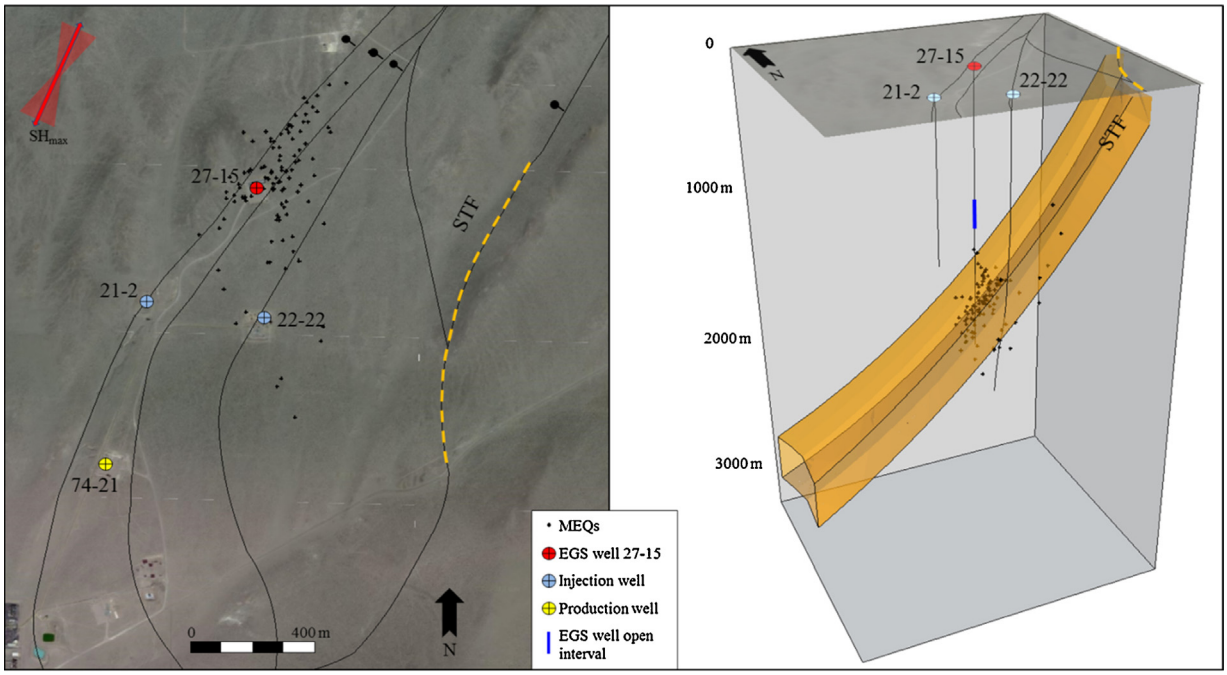

Fig. 19. Map and 3D view of the induced microseismicity observed between January 15–20, 2013. Over this period, the EGS well 27-15 extended open interval is being stimulated. The events appear located around well 27-15 and at the depth of the STF (*Shearing Target Fault*, discussed in Section 3). S_{Hmax} direction inferred from observation of borehole failures in well 27-15 (Davatzes and Hickman, 2009; Hickman and Davatzes, 2010). Black lines show surface trace of interpreted faults (Faulds et al., 2012a,b); larger black dots shown on downthrown sides of normal faults.

can undergo shear failure under the April 2011 injection-induced hydraulic pressure conditions. This 1 MPa pressure increase is consistent with observations made at the Geysers EGS Demonstration project, where pressure changes of about 1 MPa caused induced seismicity at depth and defined the outer part of the stimulation zone (Rutqvist et al., 2015) A range of 0.7–1.4 MPa induced pressure change (increasing with depth) was also found to be critical for activating shear deformation on fractures within fault zones (Jeanne et al., 2015).

Whether the observed injectivity gain is associated with (a) STF shearing processes, or (b) fracture dilation or fracturing processes in the vicinity of the wellbore (thermally and/or hydraulically-induced), needs to be verified and is part of a parallel study.

The parameters under which the model simulates this process for the April 2011 medium flow-rate phase are listed in Tables 1 and 3. The selected STF friction angle (Table 1) provides the most realistic results; higher values involve no shear deformation on the STF, while lower values cause too large a failing STF surface. Future modeling work may attempt to further calibrate the simulated shear deformation with the magnitude of the observed microseismicity, in order to better constrain the model parameterization and the extent of reservoir volumes affected by plastic deformation.

The identified STF satisfies some of the conditions that are necessary for shear failure initiation: (1) adequate initial transmissivity, and (2) optimum orientation with respect to the local stress state (McClure and Horne, 2013a,b). The initial STF transmissivity may be further enhanced by slip (McClure and Horne, 2013a,b). Related physical processes have been inferred in several injection-disposal operations, especially along faults that transit between basement rocks and overlying aquifers. Such a process may have been responsible for the recent observation of injection-induced seismicity at Guy, Arkansas (Horton, 2012). Several studies show that the injection-induced fluid pressurization can propagate through the reservoir at a kilometer scale and generate seismic events with time (including fault reactivation) (Izadi and Elsworth, 2015; Jeanne et al., 2014a,b,c; Taron et al., 2014). The injected fluid pressure diffusion and fluid migration from the formation surrounding this shallow open-hole section toward the deeper reservoir might also have been facilitated by: (a) downward migration of cooler (denser) injected fluids (Jeanne et al., 2014c; Taron et al., 2014), (b) natural fracture networks characterized by higher N-S and vertical permeability (Benato et al., 2013), and (c) leakage through the cement plug at the base of the shallow open-hole section or through the drilling-induced damage in the formation. A further element of note is that the pressure required to trigger slip on pre-existing fractures may decrease with depth (Pine and Batchelor, 1984).

The core theories of this study were laid out in the summer of 2012 (Benato et al., 2013). Well 27-15 was afterwards re-completed to the original depth (about 1770 m) in November 2012 and a new, full-hole stimulation phase was performed between January and March 2013 (Hickman et al., 2013). Further injectivity gains (more than 10-fold increase since initial, pre-EGS conditions) associated with more than 200 MEQs were observed during this latest stimulation phase (Hickman et al., 2013). The MEQs recorded during the 2013 extended open-hole section stimulation and during the previous shallow 2010/11 stimulation operations both display analogous orientation and location at depth (Fig. 19). It appears that the 2013 extended open-hole section stimulation improved access to the deeper STF discussed in this study. Direct stimulation of the STF might have provided the final desired commercial injectivity, suggesting that targeting the STF was a key decision in the stimulation plan. This investigation is part of a parallel study.

Thermal stresses and thermal damage may also have been generated by the injection of cooler fluid during the April 2011 stimulation phase. Thermal effects (and potential injectivity reversibility) during the September 2010 low flow-rate phase are discussed in Danko et al. (2012), Dempsey et al. (2013) and McClure and Horne (2013a,b). Thermal effects are considered when modeling all stages of the Desert Peak EGS stimulation as part of the ongoing FLAC3D-TOUGHREACT study, although their influence is believed to be small at the depth where the bulk of the microseis-

micity is observed; for these reasons, only isothermal simulations are carried out here. In this study, the simulation exercise is based on a comprehensive conceptual model which incorporates geological, structural and borehole data.

Given the non-uniqueness of the problem, the presented conceptual framework is one possible model for the Desert Peak EGS experiment. Coupled thermo-hydro-mechanical processes are carried out as part of a parallel study to better understand the evolution of permeability and its potential reversibility throughout the Desert Peak EGS project. The distribution of induced microseismicity seems to be controlled in a complex way by concurrent injection operations in wells 27-15 and 22-22. The conceptual framework provides a geologically reasonable model for the April 2011 Desert Peak EGS experiment in that it tests the role of the STF in focusing induced deformation manifested by MEQs. However, this type of model is inherently non-unique due to uncertainties in the geologic structure and physical properties that influence thermo-hydro-mechanical coupled processes.

Acknowledgments

This work was supported by the Desert Research Institute through a DHS fund, by the Great Basin Center for Geothermal Energy under a Geothermal Technology Program (GTP) Faculty Seed Grant, by Ormat Technologies, Inc., and by the Itasca Education Partnership program. The first author wishes to acknowledge Prof. Jim Faulds, Prof. Greg Pohll and Dr. Jonny Rutqvist for their comments/feedback while reviewing the document.

References

Baria, R., Jung, R., Tischner, T., Nicholls, J., Michelet, S., Sanjuan, B., Soma, N., Asanuma, H., Dyer, B., Garnish, J., 2006. Creation of an HDR Reservoir at 5000 m Depth at the European HDR Project. In: Proceedings of the 31st Workshop on Geothermal Reservoir Engineering, Stanford University, Stanford, California, January 30–February 1, 2006.

Benato, S., Reeves, D.M., Parashar, R., Davatzes, N.C., Hickman, S., Elsworth, D., Spielman, P., Taron, J., 2013. Computational Investigation of Hydro-Mechanical Effects on Transmissivity Evolution During the Initial Injection Phase at the Desert Peak EGS Project, NV. In: Proceedings of the 38th Workshop on Geothermal Reservoir Engineering, Stanford University, Stanford, California, February 11–13, 2013, SGP-TR-198.

Chabora, E., Zemach, E., 2013. Desert Peak EGS Project, Geothermal Technologies Program 2013 Peer Review, DOE Award: DE-FC6-02ID14406.

Chabora, E., Zemach, E., Spielman, P., Drakos, P., Hickman, S., Lutz, S., Boyle, K., Falconer, A., Robertson-Tait, A., Davatzes, N.C., Rose, P., Majer, E., Jarpe, S.,2012. Hydraulic stimulation of well 27-15, Desert Peak Geothermal Field, Nevada, USA. In: Proceedings of the 37th Workshop on Geothermal Reservoir Engineering. Stanford University, Stanford, California, January 30–February 1, 2012, SGP-TR-194.

Cladouhos, T.T., Osborn, W.L., Petty, S., Bour, D., Iovenitti, J., Callahan, O., Nordin, Y., Perry, D., Stern, P., 2012. Newberry volcano EGS demonstration – phase I results. In: Proceedings of the 37th Workshop on Geothermal Reservoir Engineering, Stanford University, Stanford, California, January 30–February 1, 2012, SGP-TR-194.

Cornet, F.H., 2000. Comment on 'Large-scale in situ permeability tensor of rocks from induced microseismicity'. Geophys. J. Int. 140.

Danko, G., Bahrami, D., Zheng, L., 2012. Coupled Multiflux-Tough2-Toughreact T-H-M-C model for EGS studies. In: Proceedings of the TOUGH Symposium 2012, Lawrence Berkeley Laboratory, Berkeley, California, September 17–19, 2012.

Davatzes, N.C., Hickman, S., 2009. Fractures, stress and fluid flow prior to stimulation of well 27-15, Desert Peak, Nevada, EGS project. In: Proceedings of the 34th Workshop on Geothermal Reservoir Engineering, Stanford University, Stanford, California, February 9–11, 2009, SGP-TR-187.

Dempsey, D., Kelkar, S., Lewis, K., Hickman, S., Davatzes, N., Moos, D., Zemach, E., 2013. Modeling Shear Stimulation of the Desert Peak EGS Well 27-15 Using a Coupled Thermal-Hydrological-Mechanical Simulator. In: Proceedings of the 47th US Rock Mechanics/Geomechanics Symposium, San Francisco, California, USA, June 23–26, 2013.

Faulds, J.E., Henry, C.D., 2008. Tectonic influences on the spatial and temporal evolution of the Walker Lane: an incipient transform fault along the evolving Pacific-North American plate boundary. In: Spencer, J.E., Titley, S.R. (Eds.), Ores and Orogenesis: CircumPacific Tectonics, Geologic Evolution, and Ore Deposits, 22. Arizona Geological Society Digest, pp. 437–470.

Faulds, J.E., Coolbaugh, M.F., Benoit, D., Opplinger, G., Perkins, M., Moeck, I., Drakos, P., 2010. Structural controls of geothermal activity in the Northern Hot Spring Mountains, Western Nevada: the tale of three geothermal systems (Brady's, Desert Peak, and Desert Queen). Geotherm. Resour. Counc. Trans. 34.

Faulds, J.E., Hinz, N., Kreemer, C., Coolbaugh, M., 2012a. Regional patterns of geothermal activity in the Great Basin Region, Western USA: correlation with strain rates. Geotherm. Resour. Counc. Trans. 36.

Faulds, J.E., Hinz, N.H., Siler, D.L., Coolbaugh, M.F., Queen, J.H., Zemach, E., 2013. Structural Controls on the Bradys Geothermal System, Western Nevada: Insights from Integrated Geologic, Geophysical, and 3D Characterization. In: 125th Anniversary Annual Meeting & Expo, The Geological Society of America, Denver, Colorado, USA, October 27–30, 2013.

Faulds, J.E., Ramelli, A.R., Garside, L.J., Coolbaugh, M.F., Green, H.L., 2012b. Preliminary geologic map of the Desert Peak Quadrangle, Churchill County, Nevada, Nevada Bureau of Mines and Geology Open-File Report 12-5, scale 1:24,000.

Genter, A., Cuenot, N., Melchert, B., Moeckes, W., Ravier, G., Sanjuan, R., Scheiber, J., Schill, E., Schmittbuhl, J., 2013. Main achievements from the multi-well EGS Soultz project during geothermal exploitation from 2010 and 2012. In: Proceedings of the European Geothermal Congress 2013, Palazzo dei Congressi, Pisa, Italy, June 3–7, 2013.

Genter, A., Fritsch, D., Cuenot, N., Baumgartner, J., Graff, J.J., 2009. Overview of the current activities of the European EGS Soultz project: from exploration to electricity production. In: Proceedings of the 34th Workshop on Geothermal Reservoir Engineering, Stanford University, Stanford, California, February 9–11, 2009, SGP-TR-187.

Hammond, W.C., Thatcher, W., 2004. Contemporary tectonic deformation of the Basin and Range province, western United States: 10 years of observation with the Global Positioning System. J. Geophys. Res. 109, B08403, http://dx.doi.org/10.1029/2003JB002746

Hettkamp, T., Baumgärtner, J., Baria, R., Gérard, A., Gandy, T., Michelet, S., Teza, D.,2004. Electricity Production from Hot Rocks. In: Proceedings, 29th Workshop on Geothermal Reservoir Engineering. Stanford University, Stanford, California, January 26–28, 2004.

Hickman, S., 1991. Stress in the lithosphere and the strength of active faults, U.S. National Report to the International Union of Geodesy and Geophysics 1987–1990. Rev. Geophys. 29, 759–775.

Hickman, S., Davatzes, N.C., 2010. In-situ stress and fracture characterization for planning of an EGS stimulation in the Desert Peak Geothermal field, Nevada. In: Proceedings of the 35th Workshop on Geothermal Reservoir Engineering, Stanford University, Stanford, California, February 1–3, 2010, SGP-TR-188.

Hickman, S., Davatzes, N.C., Zemach, E., Chabora, E., Lutz, S., Majer, E., Spielman, P., Robertson-Tait, A., Rose, P., Dempsey, D., Kelkar, S., Moos, D., 2013. Stress and Fracture Characterization for EGS Stimulation: The Desert Peak Project, Abstract Volume 2013. In: International Conference on EGS, Potsdam, Germany, May 27, 2013.

Holland, A., 2011. Examination of Possibly Induced Seismicity from Hydraulic Fracturing in the Eola Field, Garvin County, Oklahoma, Oklahoma Geological Survey Open-file, OF1-2011.

Horton, S., 2012. Disposal of hydrofracking waste fluid by injection into subsurface aquifers triggers earthquake swarn in central Arkansas with potential for damaging earthquake. Seismol. Res. Lett. 83 (March/April (2)).

2011. Itasca FLAC3D manual, Fast Lagrangian Analysis of Continua in 3 Dimensions – version 4.0. Itasca Consulting Group Inc., Minneapolis, MN.

Izadi, G., Elsworth, D., 2015. The influence of thermal-hydraulic-mechanical- and chemical effects on the evolution of permeability, seismicity and heat production in geothermal reservoirs. Geothermics 53, 385–395.

Jeanne, P., Rutqvist, J., Hartline, C., Garcia, J., Dobson, P.F., Walters, M., 2014a. Reservoir structure and properties from geomechanical modeling and microseismicity analyses associated with an enhanced geothermal system at The Geysers, California. Geothermics 51, 460–469.

Jeanne, P., Rutqvist, J., Hutchings, L., Singh, A., Dobson, P.F., Walters, M., Hartline, C., Garcia, J., 2015. Degradation of the mechanical properties imaged by seismic tomography during an EGS creation at The Geysers (California) and geomechanical modeling. Phys. Earth Planet. Inter. 240, 82–94.

Jeanne, P., Rutqvist, J., Vasco, D., Garcia, J., Dobson, P.F., Walters, M., Hartline, C., Borgia, A., 2014b. A 3D hydrogeological and geomechanical model of an Enhanced Geothermal System at The Geysers, California. Geothermics 51, 240–252.

Jeanne, P., Rutqvist, J., Vasco, D., Garcia, J., Dobson, P.F., Walters, M., Hartline, C., Borgia, A., 2014c. Development of a 3D hydrogeological and geomechanical model of an Enhanced Geothermal System using microseismic and ground deformation data from a 1-year injection program. In: Proceedings of the 39th Workshop on Geothermal Reservoir Engineering, Stanford University, Stanford, California, February 24–26, 2014, SGP-TR-202.

Larsen, P.H., 1988. Relay structures in a lower Permian basement-involved extensional system, East Greenland. J. Struct. Geol. 10, 3–8.

Lutz, S., Moore, J., Jones, C., Suemnicht, G., Robertson-Tait, A., 2009. Geological and structural relationships in the Desert Peak Geothermal System, Nevada: implications for EGS development. In: Proceedings of the 34th Workshop on Geothermal Reservoir Engineering, Stanford University, Stanford, California, February 9–11, 2009, SGP-TR-187.

Lutz, S.J., Hickman, S., Davatzes, N., Zemach, E., Drakos, P., Robertson-Tait, A., 2010. Rock mechanical testing in support of well stimulation activities at the Desert Peak geothermal field, Nevada. Geotherm. Resour. Counc. Trans. 34.

McClure, M., Horne, R., 2013a. Characterizing hydraulic fracturing with a tendency for shear stimulation test. In: The Society of Petroleum Engineers Annual Con-

ference and Exhibition, New Orleans, Louisiana, USA, 30 September–2 October 2013, SPE 166332-MS.
McClure, M., Horne, R.,2013b. Is pure shear stimulation always the mechanism of stimulation in EGS? In: Proceedings of the 38th Workshop on Geothermal Reservoir Engineering. Stanford University, Stanford, California, February 11–13, 2013, SGP-TR-198.
Nicholson, C., Wesson, R.L., 1990. Earthquake hazard associated with deep well injection – a report to the U.S. Environmental Protection Agency. U.S. Geol. Surv. Bull., 74.
Pine, R.J., Batchelor, A.S., 1984. Downward migration of shearing in jointed rock during hydraulic injections. Int. J. Rock Mech. Min. Sci. Geomech. Abstr. 21 (5), 249–263, 0148-9062/84.
Robertson-Tait, A., Lutz, S.J., Sheridan, J., Morris, C.L.,2004. Selection of an interval for massive hydraulic stimulation in well DP 23-1, Desert Peak East EGS project, Nevada. In: Proceedings of the 29th Workshop on Geothermal Reservoir Engineering. Stanford University, Stanford, California, January 26–28, 2004, SGP-TR-175.
Rose, P., Leecaster, K., Drakos, P., Robertson-Tait, A., 2009. Tracer testing at the Desert Peak EGS Project. Geotherm. Resour. Counc. Trans. 33.
Rothert, E., Shapiro, S.A., 2003. Microseismic monitoring of borehole fluid injections: data modeling and inversion for hydraulic properties of rocks. Geophysics 68 (2), 685–689.
Rozhko, A.Y., 2010. Role of seepage forces on seismicity triggering. J. Geophys. Res. 115, http://dx.doi.org/10.1029/2009JB007182
Rutqvist, J., Dobson, P.F., Garcia, J., Hartline, C., Jeanne, P., Oldenburg, C.M., Vasco, D.W., Walters, M., 2015. The northwest Geysers EGS demonstration project, California: pre-stimulation modeling and interpretation of the stimulation. Math. Geosci. 47, 3–26.
Schlinder, M., Baumgärtner, J., Gandy, T., Hauffe, P., Hettkamp, T., Menzel, H., Penzkofer, P., Teza, D., Tischner, T., Wahl, G., Successful hydraulic stimulation techniques for electric power production in the Upper Rhine Graben, Central Europe 2010. Proceedings World Geothermal Congress , Bali, Indonesia, April 25–29, 2010.
Shapiro, S.A., Audigane, P., Royer, J.J., 1999. Large-scale in situ permeability tensor of rocks from induced microseismicity. Geophys. J. Int. 137, 207–213.
Sherburn, S., Quinn, R., 2012. An Assessment of the Effects of Hydraulic Fracturing on Seismicity in the Taranaki Region, GNS Science Consultancy Report 2012/50, February 2012.
Shipton, Z.K., Soden, A.M., Kirkpatrick, J.D., Bright, A.M., Lunn, R.J., 2006. How thick is a fault? Fault-displacement-thickness scaling revisited. In: Abercrombie, R. (Ed.), Earthquakes: Radiated Energy and the Physics of Faulting. AGU Bulletin, pp. 193–198.
Stacey, R.W., Robertson-Tait, A., Drakos, P., Zemach, E., 2010. EGS stimulation of well 27-15, Desert Peak geothermal field, Nevada. Geotherm. Resour. Counc. Trans. 34.
Stewart, J.H., Perkins, M.E., 1999. Stratigraphy, tephrochronology, and structure of part of the Miocene Truckee Formation in the Trinity Range-Hot Springs Mountains area, Churchill County, east-central Nevada: USGS Open-File Report 99-330.
Swyer, M.W., Davatzes, N.C.,2013. Evaluating the role of the Rhyolite Ridge Fault System in the Desert Peak Geothermal Field with robust sensitivity testing through boundary element modeling and likelihood analysis. In: Proceedings of the 38th Workshop on Geothermal Reservoir Engineering. Stanford University, Stanford, California, February 11–13, 2013, SGP-TR-198.
Swyer, M.W., Davatzes, N.C.,2012. Using boundary element modeling of fault slip to predict patterns of stress perturbation and related fractures in geothermal reservoirs and explore parameter uncertainty. In: Proceedings of the 37th Workshop on Geothermal Reservoir Engineering. Stanford University, Stanford, California, January 30–February 1, 2012, SGP-TR-194.
Talwani, P., Acree, S., 1984. Pore pressure diffusion and the mechanism of reservoir-induced seismicity. Pageoph 122, 947–965.
Taron, J., Hickman, S., Ingebritsen, S.E., Williams, C., 2014. Using a fully coupled, open-source THM simulator to examine the role of thermal stresses in shear stimulation of enhanced geothermal systems. In: 48th US Rock Mechanics/Geomechanics Symposium, Minneapolis, MN, USA, June 1–4, 2014, ARMA 14-7525.
Townend, J., Zoback, M.D., 2000. How faulting keeps the crust strong. Geology 28, 399–402.
Wyborn, D., 2011. Hydraulic stimulation of the Habanero Enhanced Geothermal System (EGS), South Australia. In: 5th BC Unconventional Gas Technical Forum, April 2011. Geodynamics Limited.
Xu, T., Sonnenthal, E., Spycher, N., Pruess, K., 2004. TOUGHREACT User's Guide: A simulation program for non-isothermal multiphase reactive geochemical transport in variable saturated geologic media, Earth Sciences Division. Lawrence Berkeley National Laboratory, Univ. of California, Berkeley, California.
Zemach, E., Drakos, P., Robertson-Tait, A., Lutz, S.J., 2010. Feasibility evaluation of an "in-field" EGS project at Desert Peak, Nevada, USA. In: Proceedings of the World Geothermal Congress, Bali, Indonesia, April 25–29, 2010.